Article

Cell Reports

A Design Principle for an Autonomous Post-translational Pattern Formation

Graphical Abstract

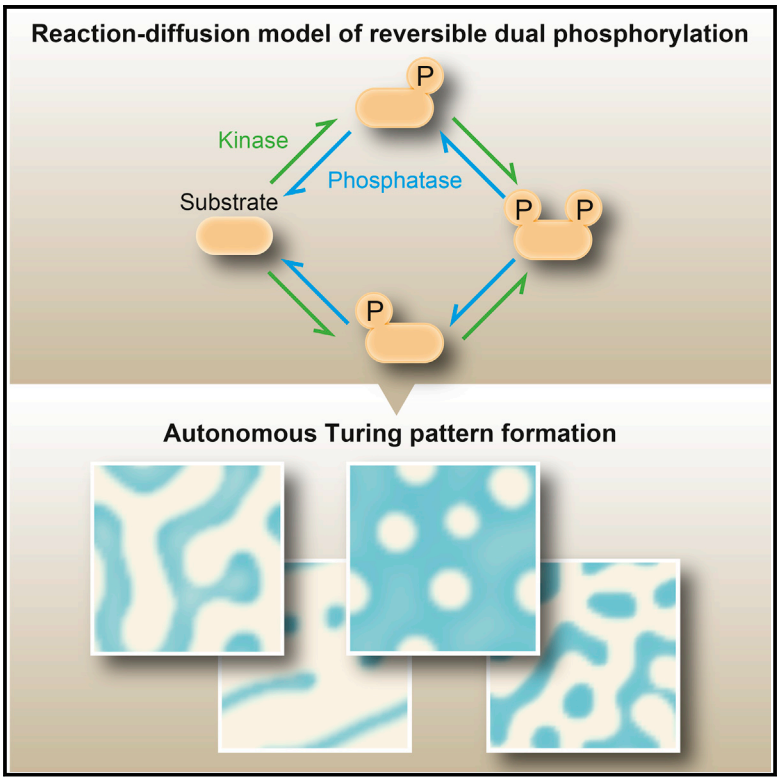

Authors

Shuhei S. Sugai, Koji L. Ode, Hiroki R. Ueda

Correspondence

uedah-tky@umin.ac.jp

In Brief

Using computer simulations, Sugai et al. showed that a generic Michaelis-Menten scheme of two-site reversible phosphorylation can produce Turing patterns in the spatial distribution of a substrate's modification states. A random parameter search found typical combinations of reaction parameters accounting for the pattern formation and tuning the pattern shapes.

Highlights

- Reversible two-site phosphorylation of a substrate can produce spatial patterns
- This design principle is mass conserved, non-autocatalytic, and non-allosteric
- Cyclic reactions with biased diffusion and enzyme sequestration are design motifs
- Stochastic simulation revealed two reaction-diffusion cycles that shape patterns

Sugai et al., 2017, Cell Reports *19*, 863–874
April 25, 2017
http://dx.doi.org/10.1016/j.celrep.2017.03.081

Cell Reports
Article

A Design Principle for an Autonomous Post-translational Pattern Formation

Shuhei S. Sugai,[1,3] Koji L. Ode,[1,2,3] and Hiroki R. Ueda[1,2,4,*]
[1]Department of Systems Pharmacology, Graduate School of Medicine, The University of Tokyo, Hongo 7-3-1, Bunkyo-ku, Tokyo 113-0033, Japan
[2]Laboratory for Synthetic Biology, RIKEN Quantitative Biology Center, 1-3 Yamadaoka, Suita, Osaka 565-0871, Japan
[3]These authors contributed equally
[4]Lead Contact
*Correspondence: uedah-tky@umin.ac.jp
http://dx.doi.org/10.1016/j.celrep.2017.03.081

SUMMARY

Previous autonomous pattern-formation models often assumed complex molecular and cellular networks. This theoretical study, however, shows that a system composed of one substrate with multisite phosphorylation and a pair of kinase and phosphatase can generate autonomous spatial information, including complex stripe patterns. All (de-)phosphorylation reactions are described with a generic Michaelis-Menten scheme, and all species freely diffuse without pre-existing gradients. Computational simulation upon >23,000,000 randomly generated parameter sets revealed the design motifs of cyclic reaction and enzyme sequestration by slow-diffusing substrates. These motifs constitute short-range positive and long-range negative feedback loops to induce Turing instability. The width and height of spatial patterns can be controlled independently by distinct reaction-diffusion processes. Therefore, multisite reversible post-translational modification can be a ubiquitous source for various patterns without requiring other complex regulations such as autocatalytic regulation of enzymes and is applicable to molecular mechanisms for inducing subcellular localization of proteins driven by post-translational modifications.

INTRODUCTION

Theoretical modeling has been a powerful tool to analyze the mechanism of autonomous pattern formation in biological systems (Karsenti, 2008; Kondo and Miura, 2010). One of the best-known models is the Turing model deploying reaction-diffusion equations (Turing, 1952). The Turing instability can arise from a system with two components, an activator with a slow diffusion rate and an inhibitor with a fast diffusion rate (Gierer and Meinhardt, 1972). The activator increases the concentrations of both the activator and the inhibitor within a short range of space, while the inhibitor represses the concentration of the activator over a long range. The detailed mechanism to realize the activation/inhibition can be varied; for example, an activator-depleted substrate scheme assumes that the inhibitory pathway is passively mediated by the insufficient supply to produce the activator (Meinhardt, 2008).

The key features underlying the Turing model have been discovered in the molecular and cellular mechanisms of biological pattern formation. At a cellular-circuit level, biological examples of the Turing model were reported in pattern formation of animal skin (Asai et al., 1999; Kondo and Asal, 1995) and in the process of vertebrate morphogenesis (Economou et al., 2012; Müller et al., 2012; Sheth et al., 2012). At a molecular-network level, a system consisting of a group of proteins called MinC, MinD, and MinE is known to show typical spatiotemporal patterns explained based on Turing instability (Raskin and de Boer, 1999; Zieske and Schwille, 2013; Loose et al., 2008). Eukaryotic cells also employ reaction-diffusion systems, including GTPase Cdc42 and kinase-substrate network of PAR proteins and atypical protein kinase C (aPKC) (Etienne-Manneville and Hall, 2002; Hoege and Hyman, 2013) as an underlying mechanism for cellular pattern formation.

Theoretical models to simulate such molecular mechanisms of pattern formation typically employed complex reaction networks (e.g., oligomerization and/or mutual inhibition among PAR proteins [Dawes and Munro, 2011; Tostevin and Howard, 2008] or cell-compartment specific activation of enzymatic activities [Alonso, 2016; Alonso and Bär, 2010, 2014; Halatek and Frey, 2012; Otsuji et al., 2007]). Alternatively, a more generic set of enzymes and substrates might be sufficient for autonomous pattern formation. Analysis using the generic but not too abstractive reaction scheme such as Michaelis-Menten scheme (Michaelis et al., 2011) allows us to compare the model parameters with the biochemically measurable values. A generic set of components to achieve reversible phosphorylation is one substrate and a kinase and a phosphatase (Kholodenko, 2006). Despite its simple setting, it has been found that reversible phosphorylation at a single substrate site can produce an ultrasensitive response in the phosphorylation state of the substrate along with a linear change of kinase/phosphatase activity (Goldbeter and Koshland, 1981). If the number of phosphorylation sites is increased, the phosphorylation status can have two or more distinct steady states (Markevich et al., 2004; Thomson and Gunawardena, 2009). It was also discovered that a traveling wave

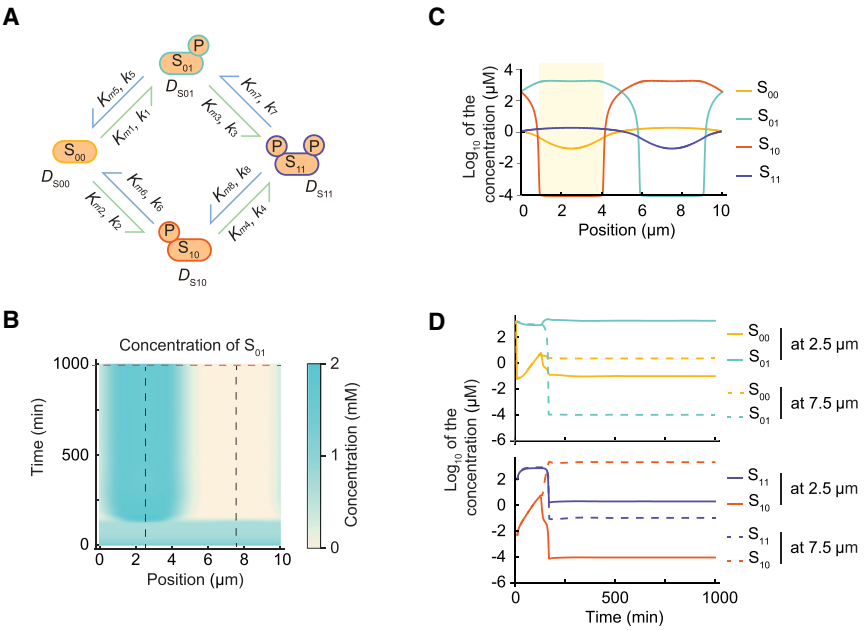

Figure 1. Autonomous Spatial Pattern Formation Arises from Reversible Dual Phosphorylation

(A) A scheme for reversible two-site phosphorylation. The enzymatic reaction follows a Michaelis-Menten reaction scheme with two parameters; k denotes the reaction speed and K_m corresponds to the inverse of enzyme-substrate affinity. Green arrow indicates the phosphorylation reaction. Blue arrow indicates the de-phosphorylation reaction.

(B) An example of pattern formation using the reaction scheme in (A). Horizontal dotted line indicates the time section at t = 1,000 min shown in (C). Vertical dotted line indicates the spatial section at the position of 2.5 and 7.5 μm shown in (D). The parameter set used in this figure is "representative parameter set for cluster 1" shown in Table S1.

(C) A section of (B) at t = 1,000 min shows the spatial pattern at the steady state. Yellow-shaded area corresponds to the S_{01} peak area, where S_{01} concentration is high.

(D) Time course of the concentration change at the position of 2.5 and 7.5 μm.

See also Figure S1 and Table S1.

(Markevich et al., 2006) and self-sustained oscillation (Jolley et al., 2012) can arise from a reversible multisite phosphorylation system. Importantly, these models of reversible multisite phosphorylation system did not assume any typical allosteric regulation of enzymes (i.e., an enzyme is regulated by a molecule that is not a direct substrate of the reaction but acts on the enzyme through a site different from a catalytic pocket or a substrate recognition site), changes in the amount of protein through protein synthesis and degradation, or any special function of enzymes and substrate (e.g., autocatalytic activity), suggesting that, under the proper combination of reaction parameters, a simple reversible phosphorylation reaction can be the core of complex and autonomous behaviors in biological systems.

A series of studies has investigated that the reversible and multisite post-translational scheme can amplify and maintain the spatial information in the presence of pre-existing patterning such as spatial compartmentalization/gradient of preferential reaction, components, and external signals (Alam-Nazki and Krishnan, 2012, 2013, 2015), or with the ability of similar reversible post-translational systems to process spatially inhomogeneous stimulus (Krishnan, 2009; Seaton and Krishnan, 2011). Nonetheless, it had been unclear whether a stable spatial pattern can autonomously arise from reversible multisite phosphorylation in the absence of any pre-existing patterning. In this study, we show that reversible two-site phosphorylation described as Michaelis-Menten-type reaction processes is sufficient for autonomous and stable spatial pattern formation. A random parameter search revealed the core mechanisms for autonomous pattern formation; local enzymatic sequestration by the interaction between enzymes and slow-diffusing substrates inhibits the production of fast-diffusing substrates. The sequestration creates an inflow of fast-diffusion substrates toward a specific area, maintaining spatial heterogeneity. Stochastic simulation further revealed the presence of two types of reaction-diffusion reaction cycles that operate to maintain a local accumulation of substrate with specific phosphorylation states.

RESULTS

Autonomous Spatial Pattern Formation Arises from Reversible Dual Phosphorylation

To construct a simple pattern-formation system, we consider a minimal model that comprises a kinase, a phosphatase, and their single substrate. It was analytically shown that, if the substrate has only one phosphorylation site, this system will always converge to a temporally and spatially uniform steady state, and a spatial pattern will not emerge autonomously (Supplemental Experimental Procedures). Therefore, we considered a dual-phosphorylation system where the two phosphorylation sites on the substrate are phosphorylated by a common kinase and de-phosphorylated by a common phosphatase (Figure 1A). In this model, the four possible modification states will be called as S_{00}, S_{10}, S_{01}, and S_{11}, respectively; S_{00} accounts for dephosphorylated substrate, S_{10} and S_{01} account for mono-phosphorylated substrate, and S_{11} accounts for di-phosphorylated substrate. Each chemical species is (de-)phosphorylated and diffuses with certain reaction and diffusion rates (Figure 1A). Mass-action kinetics is applied to one-to-one binding of enzyme and substrate and the phosphate transfer reactions. To simplify the simulation process, a Michaelis-Menten approximation is applied, but a more detailed model without this approximation will be considered in the later sections. Each substrate diffuses in one-dimensional (1D) space with circular boundary condition following Fick's law of diffusion. The 1D system size was set to 10 μm corresponding to cellular/subcellular scale. Consistent with our previous study (Jolley et al., 2012), particular parameter sets showed oscillatory behavior (Figures S1A and S1B). We

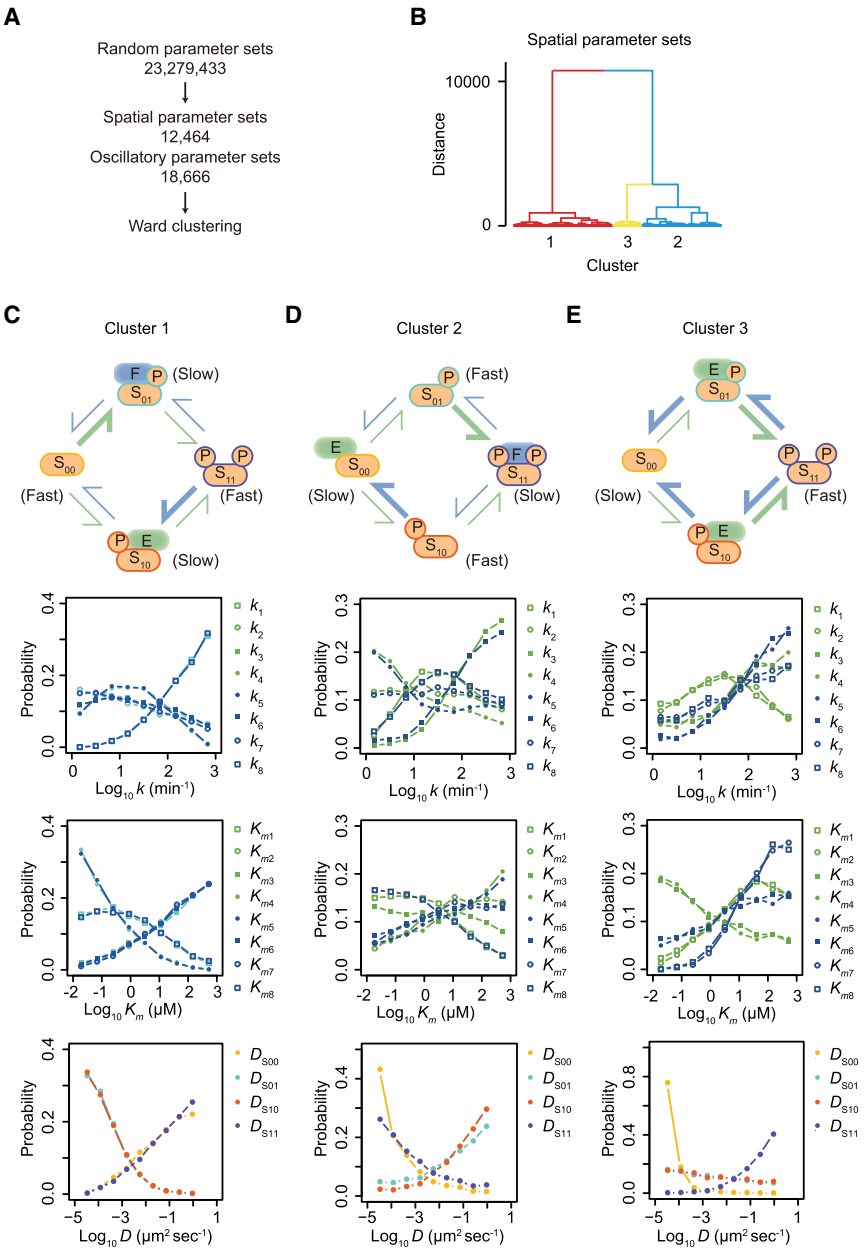

Figure 2. Three Design Motifs in Parameters for Spatial Pattern Formation

(A) Workflow for parameter motif identification.

(B) Clustering of the spatial parameter sets with Ward's algorithm.

(C–E) Parameter histograms of the spatial parameter sets. For each cluster, schematic representation is drawn at the top. Fast reactions are represented with thick arrows. Substrates with highest affinity to kinase (E) and phosphatase (F) are indicated by attaching the corresponding enzymes to the edge. Diffusion coefficients are represented as the labels "fast" or "slow."

See also Figure S2.

further found that reversible two-site phosphorylation can induce autonomous pattern formation under certain parameter combinations (Figures 1B–1D).

Three Design Motifs in Parameters for Spatial Pattern Formation

To elucidate the underlying design motifs for spatial pattern formation, a comprehensive random parameter search was conducted (Figure 2A). Reaction rate constants (k), Michaelis constants (K_m), and diffusion coefficients (D) were randomly chosen from 1–1,000 min^{-1}, 0.01–1,000 μM, and 0.001–100 $\mu m^2\ min^{-1}$ (1.67×10^{-5}-1.67 $\mu m^2\ s^{-1}$), respectively. These ranges include biochemically probable reaction and diffusion velocities based on the previous studies (Arrio-Dupont et al., 2000; Jolley et al., 2012; Markevich et al., 2004). As a result, about 0.05% and 0.08% of the total parameter sets yielded spatial patterns and oscillatory behaviors, respectively. These parameter sets were then clustered by Ward's algorithm. The reaction-diffusion scheme in our model is unchanged if the first and second phosphorylation sites are exchanged (e.g., exchanging S_{01} and S_{10}) and if the kinase and phosphatase are exchanged (e.g., exchanging S_{00} and S_{11}). To take such symmetries into account and extract qualitatively different clusters, the distance matrix for the clustering was made to incorporate symmetrical reflection and rotation. The resulting clustering dendrogram suggested the existence of two clusters for oscillatory parameter sets (Figure S2A) and three clusters for spatial parameter sets (Figure 2B).

Two clusters in oscillatory parameter sets commonly have two design motifs consistent with the previous study (Jolley et al., 2012) (Figures S2B and S2C). In brief, the biochemical system in oscillatory parameter sets tends to have clockwise cyclic reactions ($S_{00} \rightarrow S_{01} \rightarrow S_{11} \rightarrow S_{10}$). In addition, a particular substrate tends to sequestrate an enzyme due to its strong substrate-enzyme affinity, leading to synchronization of substrate states. For example, low K_{m5} results in strong binding of S_{01} to phosphatase in cluster 1. Therefore, S_{01} sequestrates phosphatase and inhibits the $S_{11} \rightarrow S_{10}$ step, leading to synchronization of substrate states at S_{11}. Cluster 2 can be interpreted as a 90-degree rotation of cluster 1. These "reaction" and "binding" motifs found in the oscillatory clusters are similarly conserved in spatial clusters 1 and 2 (Figures 2C and 2D). Notably, a bias of diffusion rates was found in spatial parameter sets ("diffusion" motif) but not in oscillatory parameter sets. To further investigate the roles of the three design motifs in spatial pattern formation, we focus on cluster 1 in the following sections without much loss of

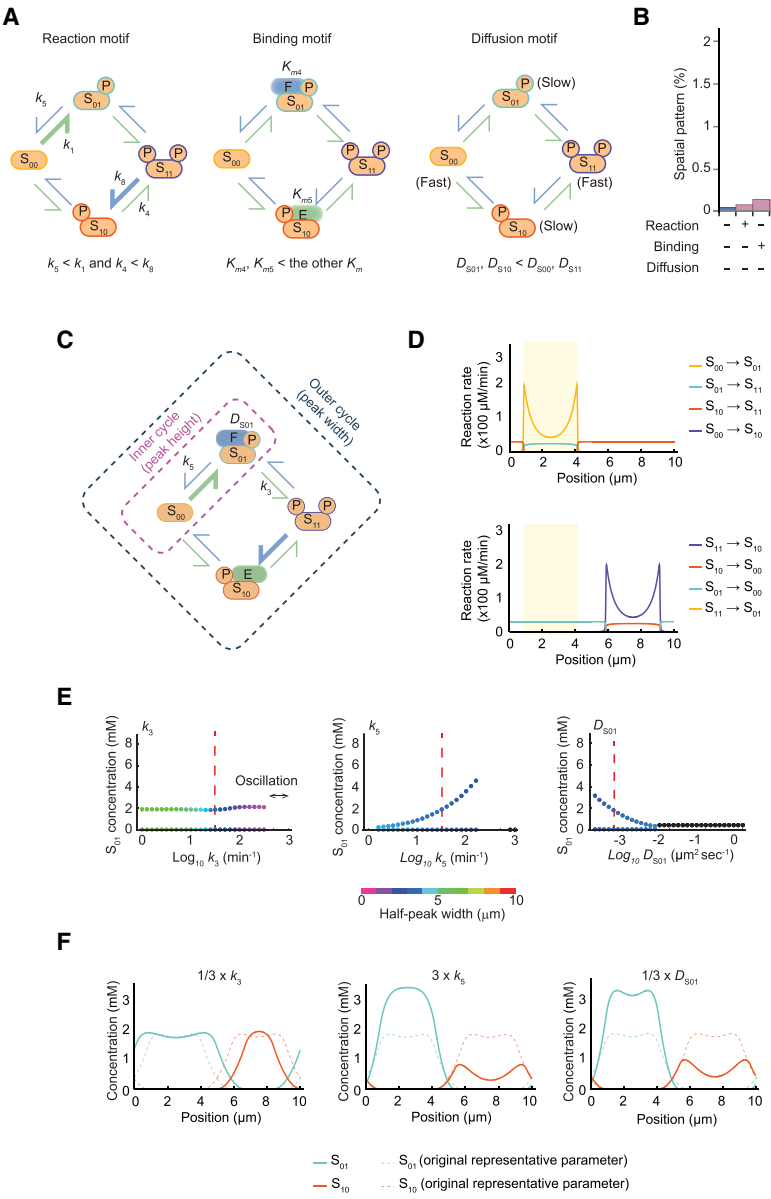

Figure 3. Inner and Outer Reaction-Diffusion Cycles Account for Peak Shape

(A) Schematic representation of reaction motif (k) for cyclic reaction direction, binding motif (K_m) for enzymatic sequestration, and diffusion motif (D) for biased diffusion velocity.

(B) Applying a constraint on the condition(s) of random parameter search corresponding to the three design motifs improves the rate of finding parameter sets for spatial pattern formation.

(C) Schematic representation of the "inner" and "outer" cycles.

(D) Spatial distribution of kinase-driven reaction rates (upper half) and phosphatase-driven reaction rates (lower half) at the steady state of spatial pattern formation. The simulation is conducted using the representative typical parameter set for spatial cluster 1 (Table S1). The yellow-shaded area corresponds to the S_{01} peak area.

(E) Three significant pattern-determining factors (k_3, k_5, and D_{S01}) were altered one by one in bifurcation analyses from the original values in the representative parameter set shown by the red dotted lines. For each value on the horizontal axis, the two dots represent the peak and trough concentration of S_{01} in the resultant spatial pattern. The color of the dots stands for the width of the peak. Black dot means spatially uniform steady state. "Oscillation" indicates the presence of temporal oscillation. In the other parameter areas with no dot or indication, the calculation failed (diverged) probably because the parameter value is close to the bifurcation point.

(F) Example distributions of substrates arising from modified parameter sets. The indicated parameter was either increased 3-fold or decreased to one-third compared with original representative parameter set.

See also Figure S3 and Table S1.

generality because cluster 1 is the largest cluster, and because cluster 1 and its rotationally symmetric cluster (cluster 2) together account for more than 85% of all spatial parameter sets. Mechanism of pattern formation in cluster 3 (Figure 2E) will be revisited in the later section.

Necessity of Three Design Motifs

Three design motifs in cluster 1 can be represented as follows (Figure 3A). For the "reaction" motif, reaction rates (k_1 and k_8) are biased toward the clockwise direction. For the "binding" motif, Michaelis constants (K_{m4} and K_{m5}) are biased to promote kinase sequestration by S_{10} and phosphatase sequestration by S_{01}, preventing the other species from binding the enzymes. For the "diffusion" motif, diffusion rates (D) of the enzyme-sequestrating substrates (i.e., D_{S01} and D_{S10}) are extremely slow, while those of the other substrates (i.e., D_{S00} and D_{S11}) are fast. Biased parameter searches with constraints reflecting these motifs resulted in an improved hit rate for spatial patterns (Figure 3B). When all three types of bias were implemented, the hit rate synergistically increased to as much as 1.86%, a more than a 30-fold increase from the original rate, suggesting that these three design motifs work cooperatively in spatial pattern formation.

Inner and Outer Reaction-Diffusion Cycles Account for Peak Shape

To elucidate the underlying reaction-diffusion mechanism of spatial pattern formation, we investigated a representative stereotypical parameter set belonging to spatial cluster 1 (Table S1). There are two characteristic areas in the steady-state distribution, where S_{01} and S_{10} are abundant (i.e., S_{01} and S_{10} peak areas) (see Figure 1C). As expected from the distribution pattern, certain reactions tend to occur in a limited range of space at the steady state (Figure 3D). By inspecting such spatially restricted reactions, we

hypothesized that there are two types of reaction-diffusion cycles, namely, the "inner" and "outer" cycles (Figure 3C). The "inner" cycle can be defined by $S_{01} \rightarrow S_{00} \rightarrow S_{01}$ (occurring at the yellow shaded area in Figure 3D). Once an S_{01} substrate is converted to S_{00}, S_{00} eventually returns to S_{01} and closes the "inner" cycle, since there is almost no reaction in the direction of $S_{00} \rightarrow S_{10}$ throughout 1D space. We also note that another "inner" cycle can be similarly defined by $S_{10} \rightarrow S_{11} \rightarrow S_{10}$.

On the other hand, the "outer" cycle can be defined by $S_{01} \rightarrow S_{11} \rightarrow S_{10} \rightarrow S_{00} \rightarrow S_{01}$. This "outer" cycle starts from the reaction $S_{01} \rightarrow S_{11}$ that predominantly occurs at the S_{01} peak area (Figure 3D, $S_{01} \rightarrow S_{11}$). Note that there is almost no reaction of the direct conversion of $S_{11} \rightarrow S_{01}$ throughout 1D space. Then, S_{11} likely undergoes a transportation from S_{01} peak area to S_{10} peak area, because S_{11} is abundant at the S_{01} peak area and depleted at the S_{10} peak area (Figure 1C). The subsequent reaction $S_{11} \rightarrow S_{10}$ occurs at the S_{10} peak area (Figure 3D, $S_{11} \rightarrow S_{10}$). A similar explanation is applicable for the reaction-diffusion process $S_{10} \rightarrow S_{00} \rightarrow S_{01}$.

To extract the decisive parameters for peak height and width, we conducted comprehensive bifurcation analyses (Figures 3E and S3). We found three parameters (k_3, k_5, and D_{S01}) (Figure 3E) and their symmetrical counterparts (k_6, k_4, and D_{S10}) (Figure S3A) are markedly important for determining peak height and width. For example, a reaction parameter (k_3) of the first reaction in the "outer" cycle largely affects peak width in a negative manner (Figure 3F, left). On the other hand, parameters (k_5, and D_{S01}) involved in the "inner" cycle largely affects peak height: diffusion of S_{01} (D_{S01}) attenuates the "inner" cycle by facilitating the outflow of S_{01} from its peak, and its decrease leads to a higher peak (Figure 3F, right). Similarly, peak growth is also facilitated by attenuating the outflow of S_{01} from its peak by accelerating k_5 (Figure 3F, middle). In summary, stimulation of the "outer" cycle carries substrates away from S_{01} peak to the other area, leading to a narrower peak. By contrast, stimulation of the "inner" cycle keeps substrates inside the peak and leads to a higher peak.

Stochastic Simulations Directly Track the "Inner" and "Outer" Reaction-Diffusion Cycles

To validate the existence of "inner" and "outer" cycles, we next aimed to directly observe the biochemical mechanisms underlying the spatial pattern formation by conducting a simulation using a stochastic simulation algorithm (SSA) (Gillespie, 1977), which can track individual molecules and their reactions at each position and time. Note that substrate-free enzymes and substrate-enzyme complexes are not explicitly considered in the presence of Michaelis-Menten approximation. To conduct SSA simulations, representative parameter set for cluster 1 was converted to mass-action parameters without Michaelis-Menten approximation (Table S2). For the sake of simplicity, all diffusion rates for substrate-free enzymes and all types of enzyme-substrate complexes are chosen to be the center of the parameter range used for random parameter search (i.e., 0.01667 $\mu m^2\ s^{-1}$).

With this setting, the total number of molecules was changed to search for the minimal number of molecules that can yield a spatial pattern (Figure 4A). A simulation with 100 enzyme and 150,000 substrate molecules results in a stable spatial pattern that remains at the same spatial position for nearly 1,000 min. The distribution of each substrate averaged throughout 100 min of simulation time with SSA (Figure S4A, left column) is mostly similar to those of the deterministic partial differential equation (PDE) (see Figure 1C). In addition, diffusion rates of substrate-free enzymes and enzyme-substrate complexes do not qualitatively change the steady-state spatial pattern at least for the representative parameter set, suggesting that the spatial pattern formation observed in the PDE model is not an artifact caused by Michaelis-Menten approximation (Figure S4B). Surprisingly, spatial pattern is still visible in the simulation with a single enzyme and 100 substrate molecules. Although the peak position of S_{01} fluctuates, the distribution pattern across 1D space at defined time shows a spatial heterogeneity qualitatively different from random noise arising from a parameter set without any design motifs for spatial pattern formation (Figures 4A and 4B). Because many reaction events are required to calculate the histogram of reaction rates, we analyzed the simulation with 100 enzyme and 150,000 substrate molecules in the following analysis. Nevertheless, the observed pattern formation with a small number of enzyme and substrate molecules suggests that pattern formation by reversible multisite phosphorylation can effectively work in subcellular compartments with a limited number of molecules.

To verify the existence of the "inner" and "outer" cycles, we next calculated the distribution of each enzymatic reaction and diffusion events in the SSA simulation (Figure S4A). Detailed inspection of these distributions confirmed the existence of the "inner" and "outer" cycles (Figure 4C). For example, $ES_{00 \rightarrow 01}$ and $FS_{01 \rightarrow 00}$ are both enriched within the S_{01} peak area (Figure S4A, left column), which corresponds to the "inner" cycle ($S_{01} \rightarrow S_{00} \rightarrow S_{01}$) predominant in S_{01} peak area. On the other hand, the first half of the "outer" cycle ($S_{01} \rightarrow S_{11} \rightarrow S_{10}$) starts at S_{01} peak area with the formation of $ES_{01 \rightarrow 11}$ to produce S_{11} (Figure S4A, left column). The fast-diffusing S_{11} is then transported from the S_{01} peak area to the S_{10} peak area (Figure S4A, right column) and results in $FS_{11 \rightarrow 10}$ formation, leading to S_{10} production (Figure S4A, left column). Similarly, the second half of the "outer" cycle ($S_{10} \rightarrow S_{00} \rightarrow S_{01}$) continues at the S_{10} peak area with the formation of $FS_{10 \rightarrow 00}$ to produce S_{00} (Figure S4A, left column). The fast-diffusing S_{00} is then transported from S_{10} peak area to S_{01} peak area (Figure S4A, right column) and results in $ES_{00 \rightarrow 01}$ formation, leading to S_{01} production (Figure S4A, left column).

To more directly observe the "inner" and "outer" cycles, we tracked a single molecule over a long trajectory (Figure 4D). When an S_{01} molecule is converted to S_{00}, the subsequent enzymatic reaction is almost always the conversion to S_{01} inside S_{01} peak area ("inner" cycle). On the other hand, when the S_{01} molecule is converted to S_{11}, the subsequent S_{10} production tends to occur outside the S_{01} peak area (the first half of the "outer" cycle).

Three Design Motifs Cooperatively Contribute to the "Inner" and "Outer" Cycles to Generate Spatial Pattern

We then sampled 200 trajectories in the representative parameter set. In the case of trajectories for S_{11} and S_{00} molecules, there are four possible trajectories as shown in Figure 5A. The trajectories other than the "inner" and "outer" cycles are termed as "other pathways." The re-production of S_{01} through the "inner" cycle ($S_{01} \rightarrow S_{00} \rightarrow S_{01}$) mostly occurs within the S_{01} peak

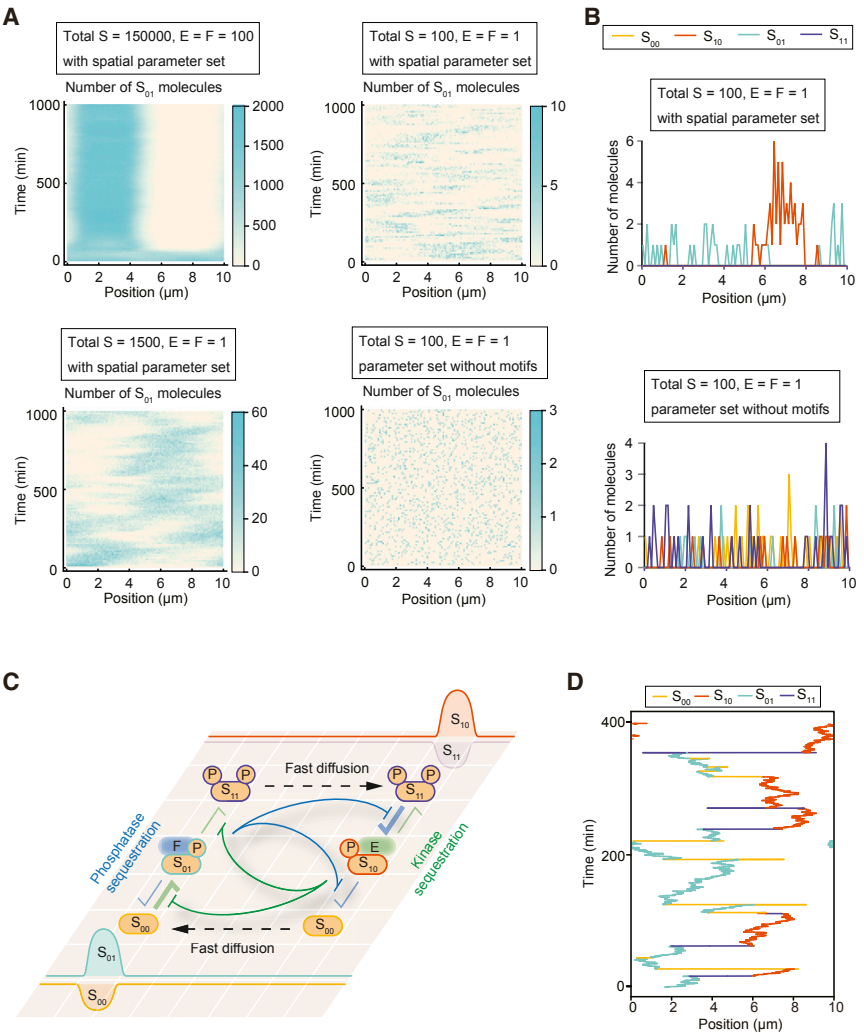

Figure 4. Stochastic Simulations Directly Track Inner and Outer Reaction-Diffusion Cycles

(A) Time evolution of S_{01} concentration based on the stochastic simulation. Total number of molecules altered in three ways as shown in the black box (top left, top right, and bottom left). A simulation with a parameter set that does not retain any motifs for spatial parameter set is also shown in the bottom right.

(B) Distribution of each substrate at $t = 100$ min with the indicated condition for the total amount of substrate and enzymes and the parameter set.

(C) Overall event following the "inner" and "outer" cycles. The cyclic reaction bias and enzyme sequestration underlie the mutually exclusive relationship between S_{01} and S_{10}. Phosphatase sequestration by S_{01} inhibits the production of S_{10} and S_{00} in the S_{01} peak area. Absence of S_{10} in this area allows the use of kinase to produce S_{01} from S_{00}, to further promote the phosphatase sequestration. The efficient consumption of S_{00} creates a concentration gradient that promotes the influx of fast-diffusing S_{00} from the surrounding area. A similar story is valid for the symmetrical S_{10} peak.

(D) Single-molecule trajectory based on the stochastic simulation with spatial parameter set.

See also Figure S4 and Table S2.

area (Figure 5B). On the other hand, the first half of the "outer" cycle ($S_{01} \rightarrow S_{11} \rightarrow S_{10}$) starts in the S_{01} peak area but ends in the S_{10} peak area (Figure 5B).

The essential roles of "reaction," "binding," and "diffusion" motifs were examined by removing each one of them from the stochastic simulation model (Table S2). The model without the "reaction" motif failed to generate spatial patterns, with the position of each unit reaction having become totally random (Figure 5C). Furthermore, all reactions were restricted to the "inner" cycle in this simulation. A similar result was observed when the "diffusion" motif was removed (Figure 5D). These results indicate that both "reaction" and "diffusion" motifs are required for the establishment of the "outer" cycle ($S_{01} \rightarrow S_{11} \rightarrow S_{10}$). The "reaction" motif is important for the "outer" cycle, because the "outer" cycle requires high concentration of S_{01} molecule that is supported by a high reaction rate of $S_{00} \rightarrow S_{01}$ in the "reaction" motif. The "diffusion" motif is also important for the "outer" cycle ($S_{01} \rightarrow S_{11} \rightarrow S_{10}$) because the "outer" cycle requires free kinase molecules, which are easily trapped by S_{10} without a low diffusion rate of S_{10} in the "diffusion" motif.

In contrast, the model without the "binding" motif preserved the "outer" cycle but still failed to generate spatial patterns (Figure 5E). The model without the "binding" motif allows "other pathways" ($S_{01} \rightarrow S_{11} \rightarrow S_{01}$ or $S_{10} \rightarrow S_{11} \rightarrow S_{01}$), which are prohibited with spatial parameter sets, suggesting that the "binding" motif can exclude other reactions than "inner" or "outer" cycles. Note that the model without three motifs altogether led to the complete collapse of reaction order, with a similar number of reactions in every direction (Figure 5F).

Three Design Motifs Contribute to Short-Range Positive Feedback and Long-Range Negative Feedback Loops to Generate Spatial Pattern

The previous theoretical studies propose that autonomous spatial pattern formation requires a short-range positive feedback and a long-range negative feedback (Gierer and Meinhardt, 1972; Turing, 1952). In our model, the "inner" and "outer" cycles seems to act as short-range positive feedback and long-range negative feedback loops, respectively (Figure 6A). In the case of short-range positive feedback loop, S_{01} indirectly activates its own production through the "inner" cycle. In detail, the reaction $S_{00} \rightarrow S_{01}$ in the "inner" cycle is mediated by the kinase that is strongly trapped by S_{10}. Alternatively, S_{01} strongly binds to the phosphatase and effectively represses the production of S_{10} from S_{11}. Thus, S_{01} and S_{10} are mutually exclusive each other, creating a positive feedback. Because S_{01} is the slow-diffusing molecule, this positive feedback loop acts within a short range. The efficient

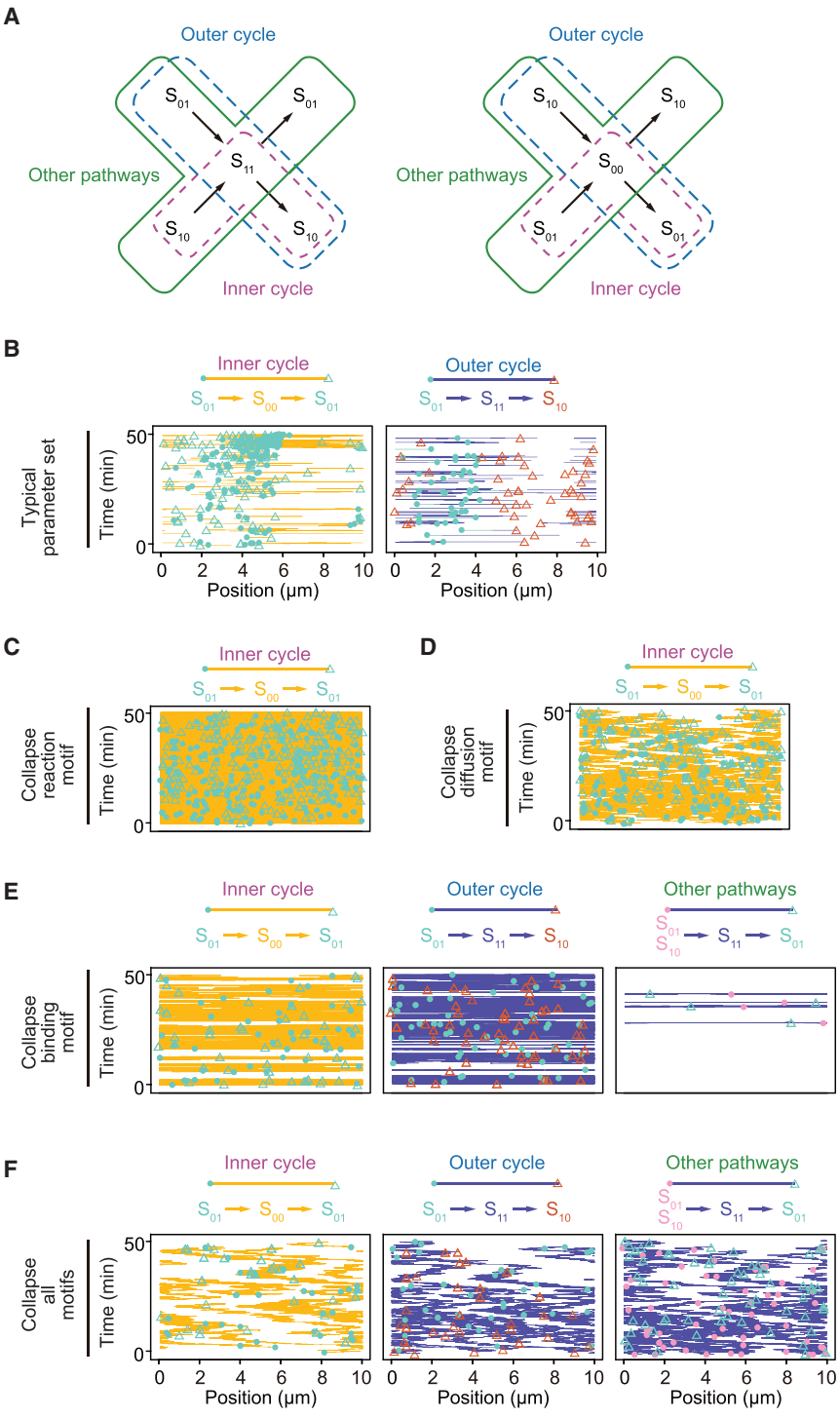

Figure 5. Three Design Motifs Cooperatively Contribute to Inner and Outer Cycles to Generate Spatial Pattern

(A) Diagrams explaining the reaction track classified as the "inner" cycle, the "outer" cycle, and "other pathways."

(B) Transition diagram of individual molecules derived from cluster 1-representative parameter set. The tracks are extracted from the reactions that occurred during 50 min in the steady state. To highlight the exclusive existence of "inner" and "outer" cycle and the absence of any other transitions, only the transitions following the triplet order shown in the box are selected for drawing. For each pathway, the fast-diffusing species' movements are represented as the lines, whose starting and ending points are shown as dots and triangles, respectively. In this condition, no reaction was found to follow the "other pathways."

(C–F) The parameter sets are changed to the ones with collapsed motifs. For (C) and (D), there are no transitions in the direction of the "outer" cycle and "other pathways."

See also Table S2.

$S_{00} \rightarrow S_{01}$ reaction promotes the consumption of S_{00} at this area. The S_{00} gradient results in the inflow of fast-diffusing S_{00} toward the S_{01} peak area, further promoting the $S_{00} \rightarrow S_{01}$ reaction. In the case of a long-range negative feedback loop, we can assume two types of antagonizing effect to the production of S_{01}. The first type is the depletion of fast-diffusing substrate molecule S_{00}. Indeed, the level of S_{01} production is suppressed at the center of S_{01} (Figure 3D), and, when the width of S_{01} increased, the S_{01} maxima started to split apart (Figure 3F). This behavior is typically observed in an activator-depleted substrate model (Meinhardt, 2008). The second type is the indirect suppression of S_{01} production through the "outer" cycle. In detail, S_{01} indirectly activates the production of S_{10} through the "outer" cycle, in which S_{01} is first converted to S_{11} in the S_{01} peak area. S_{11} then diffuses rapidly from S_{01} peak area to S_{10} peak area. In the S_{10} peak area, S_{11} is eventually converted into S_{10}. Since S_{10} strongly binds to a kinase and effectively represses S_{01} production from S_{00}, the "outer" cycle can form the negative feedback loop for S_{01}. Because S_{11} is the fast-diffusing molecule, this negative feedback loop acts over a long range.

A Reversible Two-Site Modification Model Can Generate Complex Pattern Formation in Two-Dimensional Space

The Turing mechanism is well known to elicit various spatial patterns when it operates in two-dimensional (2D) space. To verify the potential of a reversible two-site modification model, we extended our simulation in 2D space with periodic boundary condition. The area was set to 900 μm^2 corresponding to the order of eukaryotic cell membrane (Kholodenko et al., 2000). Because a representative parameter set in cluster 1 has a symmetric and mutually

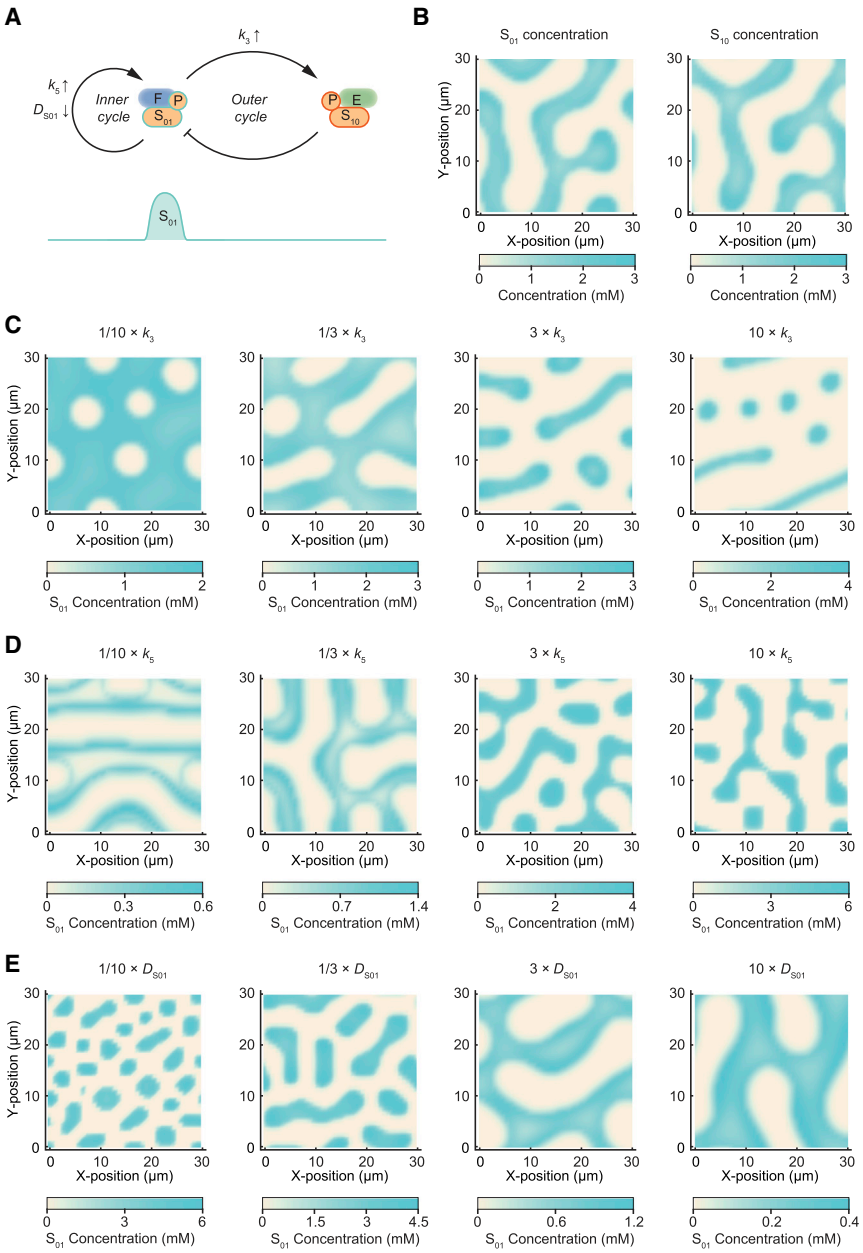

Figure 6. A Reversible Two-Site Modification Model Can Generate Complex Pattern Formation in 2D Space

(A) The "inner" cycle with phosphatase sequestration contributes to the short-range positive feedback for the production of S_{01}. The "outer" cycle with kinase sequestration contributes to long-range negative feedback for the production of S_{01}.

(B) 2D patterns from cluster 1-representative parameter set.

(C–E) Modifying one of the parameters in the cluster 1-representative parameter set resulted in various pattern shapes. Only the distributions of S_{01} are shown. Changes in k_3 predominantly affect the peak width. The maximum concentration of S_{01} is altered significantly with k_5 and D_{s01} (see the concentration shown below each 2D plot).

See also Figure S5 and Table S1.

exclusive relationship between S_{01} and S_{10}, it exhibited a stripe pattern when it operates in 2D space, where S_{01} and S_{10} complementarily occupied the space with almost identical stripe width and peak concentration (Figure 6B). When we changed the value of k_3, the critical parameter for the "outer" cycle and hence for peak width, the spatial pattern in 2D space was greatly affected: the increase of k_3 resulted in the decreased stripe width and ended up with the fragmented dots of high S_{01} regions (Figure 6C). Along the 100-fold change in k_3 value, the peak value of S_{01} was less affected. On the other hand, changes in k_5 and D_{S01}, parameters responsible for the "inner" cycle, and hence the peak height had more impact on the peak concentration of stripe. The 100-fold increase in the k_5 value and 100-fold decrease in the D_{S01} value changed the peak concentration almost 10-fold (Figures 6D and 6E), while it did not affect the stripe width much. A similar mechanism of pattern formation is likely to take place for the parameter sets of cluster 2 (Figure S5).

Breakdown to the Minimal Requirement for Spatial Pattern Formation

The remaining cluster 3 had horizontal reflection symmetry (i.e., the overall parameter distribution is unchanged by exchanging the position of S_{01} and S_{10}) (Figure 2E). Even when one of the two mono-phosphorylated substrates was omitted from the scheme (Figure 7A), the model with three modification states (i.e., S_0, S_1, and S_2) exhibited spatial pattern formation. A random parameter search revealed one cluster for the spatial parameter set (Figure 7B). Parameter distribution of the cluster was almost the same as what was obtained by eliminating one of the mono-phosphorylated forms from spatial cluster 3 in the four-modification-state model (cf. Figures 2E and 7C). Therefore, spatial cluster 3 in the four-state model seems a superimposed version of two three-state models.

A core feature of design motifs as well as mechanism of pattern formation found in the four-state model is conserved in the three-state model: there is a clear reaction bias to produce the slow-diffusion species (S_0) from the fast-diffusion species (S_2). Based on the parameter distribution (Figure 7C), we created a representative parameter set for this three-state model (Table S3). A steady-state distribution of substrate concentration and reaction rates (Figure 7D) indicated that the slow-diffusing species S_0 amplifies its own synthesis via the inflow of the

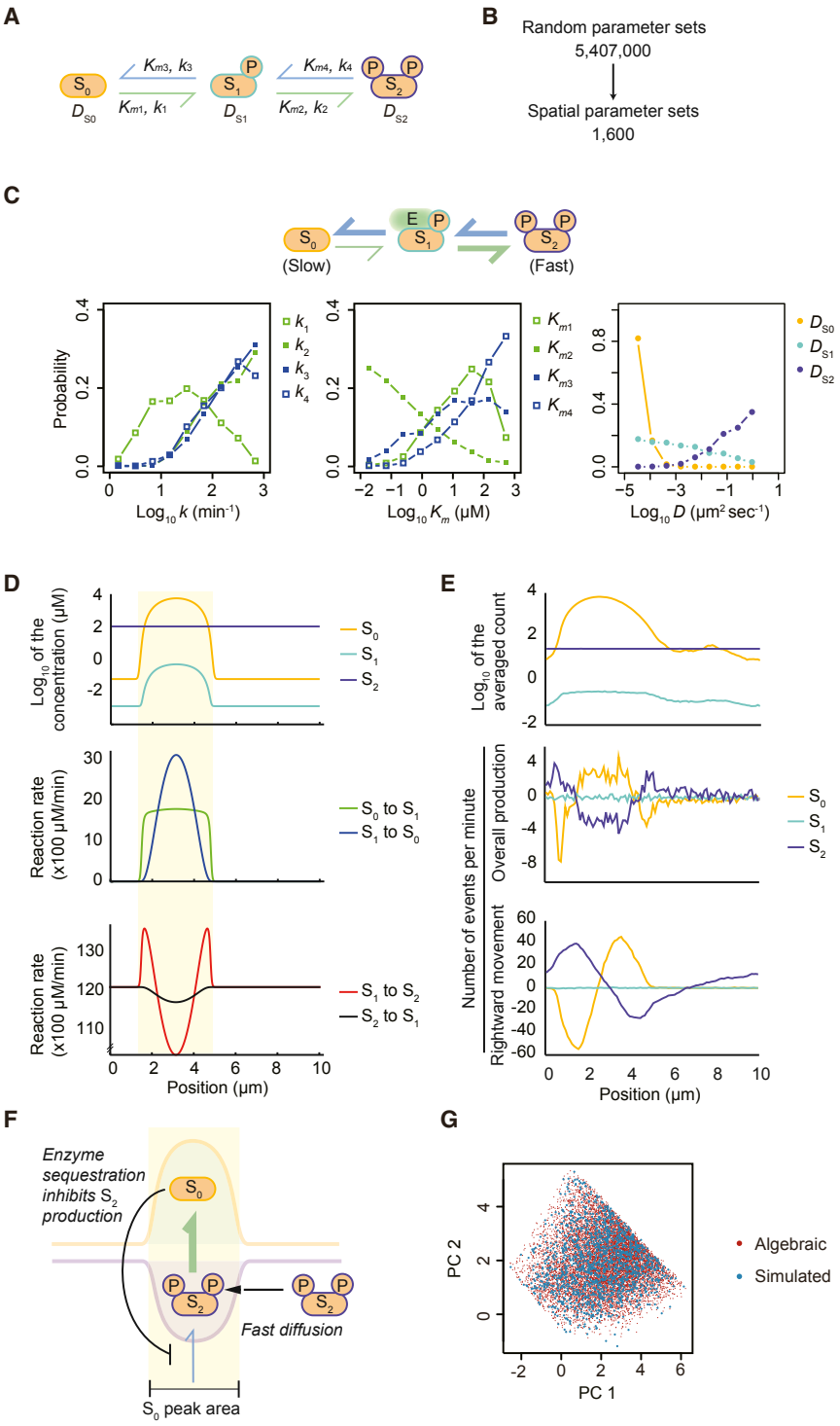

Figure 7. Breakdown to the Minimal Requirement for Spatial Pattern Formation

(A) Three-state reaction scheme.

(B) Workflow to derive the condition for spatial pattern formation.

(C) Parameter histograms for the spatial parameter set and schematic representation of spatial parameter set in three-state model.

(D) Spatial pattern arising from the representative parameter set for three-state model. Concentration of each substance (top), reaction rate involving kinase (middle), and phosphatase (bottom) are plotted for each position. The shaded area corresponds to the S_0 peak area. See Table S3 for the representative parameter values.

(E) Result from stochastic simulation with the three-state scheme and the total initial number S = 150,000, E = F = 100. Averaged distribution (top), overall production rate (middle), and overall rightward movement (bottom) are shown for each bin position. Distribution was averaged for 100 min after the establishment of spatial pattern. In the same time frame, overall production rate and overall movements were calculated in the same manner as in Figure S4A. See Table S4 for the parameter values.

(F) Schematic expression of the spatial pattern maintenance. Kinase sequestration by S_0 at the center of the peak and its release at the peripheral area, and overall absorption of substance in the form of fast-diffusing S_2 are depicted.

(G) Parameter sets that met algebraic conditions for Turing instability (red) and that produced spatial patterns in the simulation (blue) are projected on the same principle component (PC) space.

See also Figure S6 and Tables S3 and S4.

fast-diffusing species S_2 (Figure 7E). At the center of S_0 peak, the overwhelming amount of S_0 sequestrates the kinase, inhibiting $S_1 \rightarrow S_2$. This makes the overall reaction inclined toward $S_2 \rightarrow S_1 \rightarrow S_0$, and S_2 concentration tends to be lower. Following this gradient, fast-diffusing S_2 flows into the center of S_0 peak that further stimulates the production of S_0 (Figure 7F). Like the case of four-state model, the long-range negative feedback in the three-state model can be interpreted as activator-depleted scheme (Meinhardt, 2008): slow-diffusing S_0 is produced from fast-diffusing S_2 and production rate of S_2 at the center of S_0 is suppressed.

An apparent difference in the parameter distribution between the three-state model and the four-state model lies in the binding affinity of substrate and enzyme. In the four-state model, the highest substrate-enzyme affinity lies in a slow-diffusion substrate making the peak (Figures 2C and 2D). In the three-state model, S_1, the second slowest diffusion species has the highest affinity with kinase. This represents the restriction of three-state model; n the three-state model, reproduction of S_2 requires kinase-driven phosphorylation of S_1. To this end, S_1 needs to take back kinase from S_0 at some point of reaction cascade, thus needs to have a high kinase-substrate affinity.

The simplicity of this three-state model enabled an analytical approach using linear stability analysis (Supplemental

Experimental Procedures). One requirement for the emergence of spatial pattern is that the phosphorylation and de-phosphorylation of two sites are carried out by the same kinase and phosphatase, indicating the importance of enzymatic sequestration to affect other reaction steps sharing the same enzyme. Furthermore, analytical examination revealed the requirements of the parameter sets to have a potential to generate spatial patterns by amplifying small fluctuations in an almost homogeneous 1D space. The parameter space satisfying such analytic requirements are closely overlapped with the parameter space that resulted in spatial pattern formation in numerical simulation, implying the validity of this analytical approach (Figure 7G).

Unlike clusters 1 and 2, cluster 3 does not have a mutually exclusive relationship between two species (e.g., S_{01} and S_{10} in cluster 1). Therefore, there is no constraint to partition the 2D space for the two antagonizing species. This relaxed constraint leads to a single peak pattern even in the 2D space. The width of resultant peak was tunable from a small single dot to a more blurred concentration gradient (Figure S6).

DISCUSSION

Comparison with Other Mass-Conserved Reaction-Diffusion Models for Scale-free Pattern Formation

When the total amount of substances is kept constant by assuming that no de novo synthesis and degradation of components happen, the reaction-diffusion system results in the emergence of spatial pattern with single peak in 1D space (Goryachev and Pokhilko, 2008; Ishihara and Kaneko, 2006; Otsuji et al., 2007). Under the local positive feedback for peak emergence, the highest peak consumes the resource more effectively than lower peaks, further stimulating the growth of the highest peak. The winner-take-all situation allows only one peak to survive at steady state in an entire space where the competition of limited resources effectively occurs. Consistent with the previous finding (Otsuji et al., 2007), most (>80%) of the spatial parameters found in our random parameter search in 1D space resulted in the single peak for substrate with a specific modification state.

The single peak pattern, which is resilient to the changes in the system size, was also observed in a reaction-diffusion system with a mechanism called wave-pinning (Jilkine and Edelstein-Keshet, 2011; Mori et al., 2008). In the wave-pinning system, spatially homogeneous steady state is stable, whereas in the mass-conserved Turing system, spatially homogeneous steady state is unstable and an infinitesimally small perturbation to break the homogeneity leads to the emergence of spatial pattern. The spatial pattern formation in our model belongs to the mass-conserved Turing system and not to the wave-pinning system, because part of our criteria for the screening of spatial parameter set requires Turing instability. Nonetheless, it is expected that the scheme of reversible-multisite phosphorylation can exhibit wave-pinning mechanism because the scheme is mass-conserved and can have a bistability (Markevich et al., 2004).

General Model of Pattern Formation by Reversible Two-Site Phosphorylation

Our study proposes that the reversible two-site modification of a single substrate by two competing enzymes could be the direct source for spatial pattern formation. For example, it was shown that a two-phosphorylation mitogen-activated protein kinase (MAPK) signaling forms a focus in a unicellular organism fission yeast (Dudin et al., 2016). The focalization process is assumed to involve several feedback pathways including actin stabilization, but our model suggests that the reversible phosphorylation of MAPK itself may play a role to evoke a local accumulation of the signaling pathway.

A part of "reaction," "binding," and "diffusion" motifs can be found in enzymes/substrates including mitogen-activated protein kinase kinase (MAPKK) and CKIδ/ε. These kinases phosphorylate substrates at multiple sites following a preferred order, corresponding to the cyclic bias revealed in our modeling study (Ferrell and Bhatt, 1997; Flotow et al., 1990; Vanselow et al., 2006). In these systems, previous studies have suggested that enzyme sequestration plays an important role to elicit non-linear responses (Jolley et al., 2012; Markevich et al., 2004). In these enzymes, the phosphorylation status of the substrate affects the substrate affinity through a substrate recognition site, whose interaction with the substrate is dependent on the electrostatic status of the substrate. The catalytic constant is also affected because the substrate recognition can define the conformation of the substrate toward the catalytic pocket and hence determine its catalytic constant. In this sense, our biochemical model can naturally accommodate the characteristics of these enzymes, which do not have a typical allosteric regulation. Another specific requirement for the formation of spatial patterns is a difference in diffusion rates depending on the phosphorylation state of the substrate. Although the change in molecular weight by the addition of one or two phosphate groups itself will not alter the diffusion rate of modified substrate significantly, the diffusion rate can be dramatically altered by the altered affinity of modified substrate with scaffold structures such as cytoskeletal proteins, cell membranes, and chromosomes.

Although our modeling study started without constraints based on previously identified molecular networks, the overall mechanism encompasses several key features found in other specific biological models including sequestration-based directional flow and mutual exclusion of two key species (Dawes and Munro, 2011; Halatek and Frey, 2012; Otsuji et al., 2007; Tostevin and Howard, 2008). Furthermore, our model can provide a unified view for the role of protein localization; when the substrate-enzyme complex is localized in the specific area, the role of localization may be enzyme sequestration for autonomous spatial formation rather than only enrichment of enzymatic activity. Taken together, the simplicity and generality of our reversible phosphorylation model provides a framework to investigate a biochemical source of autonomous pattern formation and ultimately, to synthesize a de novo molecular network that inherently encodes spatial information.

EXPERIMENTAL PROCEDURES

All the details of equations and simulation processes are presented in Supplemental Experimental Procedures.

Modeling the Reversible Phosphorylation with Diffusion Process

The phosphorylation and de-phosphorylation processes were described as the Michaelis-Menten scheme for enzymatic reaction, consisting of the

binding of enzyme and substrate, the dissociation of enzyme-substrate complex, and the reaction of phosphate transfer/removal. Quasi-steady-state approximation on the formation of enzyme-substrate complex (i.e., Michaelis-Menten approximation) was applied for deterministic simulations.

Random and Biased Parameter Search

For random parameter search, each reaction rate constant (k), Michaelis constant (K_m), and diffusion coefficient (D) were randomly chosen from the exponentially distributed parameters within the range of 1–1,000 min^{-1}, 0.01–1,000 μM, and 0.001–100 $\mu m^2\ min^{-1}$ (1.67×10^{-5}–$1.67\ \mu m^2\ s^{-1}$), respectively.

The obtained spatial and oscillatory parameter sets were then clustered through Ward's algorithm. The four-state model has a horizontal symmetry (e.g., exchanging the position of S_{01} and S_{10}) and a point symmetry (e.g., exchanging the role of kinase and phosphatase). A distance matrix between the parameter sets was made to cancel those inherent symmetries of the reaction scheme.

For each biased parameter search reflecting one or more of the three design motifs, randomly generated parameters that satisfied the following constraints were used for PDE calculation: (1) cyclic reaction motif: $k_5 < k_1$ and $k_4 < k_8$, (2) binding motif: Max $\{K_{m4}, K_{m5}\}$ < Min $\{K_{m1}, K_{m2}, K_{m3}, K_{m6}, K_{m7}, K_{m8}\}$, and (3) biased diffusion motif: Max $\{D_{S01}, D_{S10}\}$ < Min $\{D_{S00}, D_{S11}\}$.

Representative Parameter Set

To analyze the mechanisms of spatial pattern formation from each cluster, a representative parameter set was created to represent the tendency of the given cluster's parameter distribution. For monotonously increasing or decreasing histogram, its extreme value was adopted. For a histogram with an apparent single peak value, the peak value was adopted. For the parameters that had no significant tendency, a value around its average was adopted.

Bifurcation Analysis

The representative parameter set (four-state model, spatial cluster 1) was used for the bifurcation analysis shown in Figures 3 and S3. Each parameter was varied among the indicated range. After the system reaches steady state, peak and trough of S_{01} concentration and spatial width between two points that give half the concentration of S_{01} peak were calculated.

Stochastic Simulation

The representative parameter sets for clusters 1 and 3 and the representative parameter set for the three-state model were all converted to the full mass-action parameter sets before conducting SSA calculations. For the single-molecule tracking, 150,000 substrate molecules and only one "tagged" substrate molecule were simulated in a common environment but recorded separately.

SUPPLEMENTAL INFORMATION

Supplemental Information includes Supplemental Experimental Procedures, six figures, and four tables and can be found with this article online at http://dx.doi.org/10.1016/j.celrep.2017.03.081.

AUTHOR CONTRIBUTIONS

S.S.S., K.L.O., and H.R.U. designed the study. S.S.S. performed most of the simulation study. S.S.S., K.L.O., and H.R.U. analyzed the mechanism of pattern formation and wrote the manuscript.

ACKNOWLEDGMENTS

We thank all the lab members at RIKEN QBiC and the University of Tokyo, in particular Dr. Craig C. Jolley for assisting the computer simulation and Dr. Arthur Millius for critical reading of this manuscript. We are grateful to Drs. Shigeru Kondo, Shuji Ishihara, and Ryokichi Tanaka for valuable comments. This work was supported by a grant from AMED-CREST (AMED/MEXT, H.R.U.), CREST (JST/MEXT, H.R.U.), Brain/MINDS (AMED/MEXT, H.R.U.), Basic Science and Platform Technology Program for Innovative Biological Medicine (AMED/MEXT, H.R.U.), a Grant-in-Aid for Scientific Research (S) (JSPS KAKENHI grant number 25221004, H.R.U.), a Grant-in-Aid for Scientific Research on Innovative Areas (JSPS KAKENHI grant number 23115006, H.R.U.), the strategic programs for R&D (President's discretionary fund) of RIKEN (H.R.U.), an intramural Grant-in-Aid from the RIKEN QBiC (H.R.U.), a grant from Takeda Science Foundation, a Grant-in-Aid for Young Scientists (B) (JSPS KAKENHI grant number 25830146, K.L.O.), and a Grant-in-Aid for Challenging Exploratory Research (JSPS KAKENHI grant number 16K14653, K.L.O.).

Received: October 1, 2016
Revised: January 22, 2017
Accepted: March 30, 2017
Published: April 25, 2017; corrected online: May 4, 2017

REFERENCES

Alam-Nazki, A., and Krishnan, J. (2012). An investigation of spatial signal transduction in cellular networks. BMC Syst. Biol. *6*, 83.

Alam-Nazki, A., and Krishnan, J. (2013). Covalent modification cycles through the spatial prism. Biophys. J. *105*, 1720–1731.

Alam-Nazki, A., and Krishnan, J. (2015). Spatial control of biochemical modification cascades and pathways. Biophys. J. *108*, 2912–2924.

Alonso, S. (2016). Pattern formation at cellular membranes by phosphorylation and dephosphorylation of proteins. In Nonlinear Dynamics in Biological Systems, J. Carballido-Landeira and B. Escribano, eds. (Springer International Publishing), pp. 63–82.

Alonso, S., and Bär, M. (2010). Phase separation and bistability in a three-dimensional model for protein domain formation at biomembranes. Phys. Biol. *7*, 046012.

Alonso, S., and Bär, M. (2014). Modeling domain formation of MARCKS and protein kinase C at cellular membranes. EPJ Nonlinear Biomedical Physics *2*, 1–18.

Arrio-Dupont, M., Foucault, G., Vacher, M., Devaux, P.F., and Cribier, S. (2000). Translational diffusion of globular proteins in the cytoplasm of cultured muscle cells. Biophys. J. *78*, 901–907.

Asai, R., Taguchi, E., Kume, Y., Saito, M., and Kondo, S. (1999). Zebrafish leopard gene as a component of the putative reaction-diffusion system. Mech. Dev. *89*, 87–92.

Dawes, A.T., and Munro, E.M. (2011). PAR-3 oligomerization may provide an actin-independent mechanism to maintain distinct par protein domains in the early Caenorhabditis elegans embryo. Biophys. J. *101*, 1412–1422.

Dudin, O., Merlini, L., and Martin, S.G. (2016). Spatial focalization of pheromone/MAPK signaling triggers commitment to cell-cell fusion. Genes Dev. *30*, 2226–2239.

Economou, A.D., Ohazama, A., Porntaveetus, T., Sharpe, P.T., Kondo, S., Basson, M.A., Gritli-Linde, A., Cobourne, M.T., and Green, J.B. (2012). Periodic stripe formation by a Turing mechanism operating at growth zones in the mammalian palate. Nat. Genet. *44*, 348–351.

Etienne-Manneville, S., and Hall, A. (2002). Rho GTPases in cell biology. Nature *420*, 629–635.

Ferrell, J.E., Jr., and Bhatt, R.R. (1997). Mechanistic studies of the dual phosphorylation of mitogen-activated protein kinase. J. Biol. Chem. *272*, 19008–19016.

Flotow, H., Graves, P.R., Wang, A.Q., Fiol, C.J., Roeske, R.W., and Roach, P.J. (1990). Phosphate groups as substrate determinants for casein kinase I action. J. Biol. Chem. *265*, 14264–14269.

Gierer, A., and Meinhardt, H. (1972). A theory of biological pattern formation. Kybernetik *12*, 30–39.

Gillespie, D.T. (1977). Exact stochastic simulation of coupled chemical reactions. J. Phys. Chem. *81*, 2340–2361.

Goldbeter, A., and Koshland, D.E., Jr. (1981). An amplified sensitivity arising from covalent modification in biological systems. Proc. Natl. Acad. Sci. USA *78*, 6840–6844.

Goryachev, A.B., and Pokhilko, A.V. (2008). Dynamics of Cdc42 network embodies a Turing-type mechanism of yeast cell polarity. FEBS Lett. *582*, 1437–1443.

Halatek, J., and Frey, E. (2012). Highly canalized MinD transfer and MinE sequestration explain the origin of robust MinCDE-protein dynamics. Cell Rep. *1*, 741–752.

Hoege, C., and Hyman, A.A. (2013). Principles of PAR polarity in Caenorhabditis elegans embryos. Nat. Rev. Mol. Cell Biol. *14*, 315–322.

Ishihara, S., and Kaneko, K. (2006). Turing pattern with proportion preservation. J. Theor. Biol. *238*, 683–693.

Jilkine, A., and Edelstein-Keshet, L. (2011). A comparison of mathematical models for polarization of single eukaryotic cells in response to guided cues. PLoS Comput. Biol. *7*, e1001121.

Jolley, C.C., Ode, K.L., and Ueda, H.R. (2012). A design principle for a post-translational biochemical oscillator. Cell Rep. *2*, 938–950.

Karsenti, E. (2008). Self-organization in cell biology: A brief history. Nat. Rev. Mol. Cell Biol. *9*, 255–262.

Kholodenko, B.N. (2006). Cell-signalling dynamics in time and space. Nat. Rev. Mol. Cell Biol. *7*, 165–176.

Kholodenko, B.N., Hoek, J.B., and Westerhoff, H.V. (2000). Why cytoplasmic signalling proteins should be recruited to cell membranes. Trends Cell Biol. *10*, 173–178.

Kondo, S., and Asal, R. (1995). A reaction-diffusion wave on the skin of the marine angelfish Pomacanthus. Nature *376*, 765–768.

Kondo, S., and Miura, T. (2010). Reaction-diffusion model as a framework for understanding biological pattern formation. Science *329*, 1616–1620.

Krishnan, J. (2009). Signal processing through a generalized module of adaptation and spatial sensing. J. Theor. Biol. *259*, 31–43.

Loose, M., Fischer-Friedrich, E., Ries, J., Kruse, K., and Schwille, P. (2008). Spatial regulators for bacterial cell division self-organize into surface waves in vitro. Science *320*, 789–792.

Markevich, N.I., Hoek, J.B., and Kholodenko, B.N. (2004). Signaling switches and bistability arising from multisite phosphorylation in protein kinase cascades. J. Cell Biol. *164*, 353–359.

Markevich, N.I., Tsyganov, M.A., Hoek, J.B., and Kholodenko, B.N. (2006). Long-range signaling by phosphoprotein waves arising from bistability in protein kinase cascades. Mol. Syst. Biol. *2*, 61.

Meinhardt, H. (2008). Models of biological pattern formation: From elementary steps to the organization of embryonic axes. Curr. Top. Dev. Biol. *81*, 1–63.

Michaelis, L., Menten, M.L., Johnson, K.A., and Goody, R.S. (2011). The original Michaelis constant: Translation of the 1913 Michaelis-Menten paper. Biochemistry *50*, 8264–8269.

Mori, Y., Jilkine, A., and Edelstein-Keshet, L. (2008). Wave-pinning and cell polarity from a bistable reaction-diffusion system. Biophys. J. *94*, 3684–3697.

Müller, P., Rogers, K.W., Jordan, B.M., Lee, J.S., Robson, D., Ramanathan, S., and Schier, A.F. (2012). Differential diffusivity of Nodal and Lefty underlies a reaction-diffusion patterning system. Science *336*, 721–724.

Otsuji, M., Ishihara, S., Co, C., Kaibuchi, K., Mochizuki, A., and Kuroda, S. (2007). A mass conserved reaction-diffusion system captures properties of cell polarity. PLoS Comput. Biol. *3*, e108.

Raskin, D.M., and de Boer, P.A. (1999). Rapid pole-to-pole oscillation of a protein required for directing division to the middle of Escherichia coli. Proc. Natl. Acad. Sci. USA *96*, 4971–4976.

Seaton, D.D., and Krishnan, J. (2011). The coupling of pathways and processes through shared components. BMC Syst. Biol. *5*, 103.

Sheth, R., Marcon, L., Bastida, M.F., Junco, M., Quintana, L., Dahn, R., Kmita, M., Sharpe, J., and Ros, M.A. (2012). Hox genes regulate digit patterning by controlling the wavelength of a Turing-type mechanism. Science *338*, 1476–1480.

Thomson, M., and Gunawardena, J. (2009). Unlimited multistability in multisite phosphorylation systems. Nature *460*, 274–277.

Tostevin, F., and Howard, M. (2008). Modeling the establishment of PAR protein polarity in the one-cell C. elegans embryo. Biophys. J. *95*, 4512–4522.

Turing, A.M. (1952). The chemical basis of morphogenesis. Philos. Trans. R. Soc. Lond. B Biol. Sci. *237*, 37–72.

Vanselow, K., Vanselow, J.T., Westermark, P.O., Reischl, S., Maier, B., Korte, T., Herrmann, A., Herzel, H., Schlosser, A., and Kramer, A. (2006). Differential effects of PER2 phosphorylation: Molecular basis for the human familial advanced sleep phase syndrome (FASPS). Genes Dev. *20*, 2660–2672.

Zieske, K., and Schwille, P. (2013). Reconstitution of pole-to-pole oscillations of min proteins in microengineered polydimethylsiloxane compartments. Angew. Chem. Int. Ed. Engl. *52*, 459–462.

Cell Reports, Volume *19*

Supplemental Information

A Design Principle for an Autonomous Post-translational Pattern Formation

Shuhei S. Sugai, Koji L. Ode, and Hiroki R. Ueda

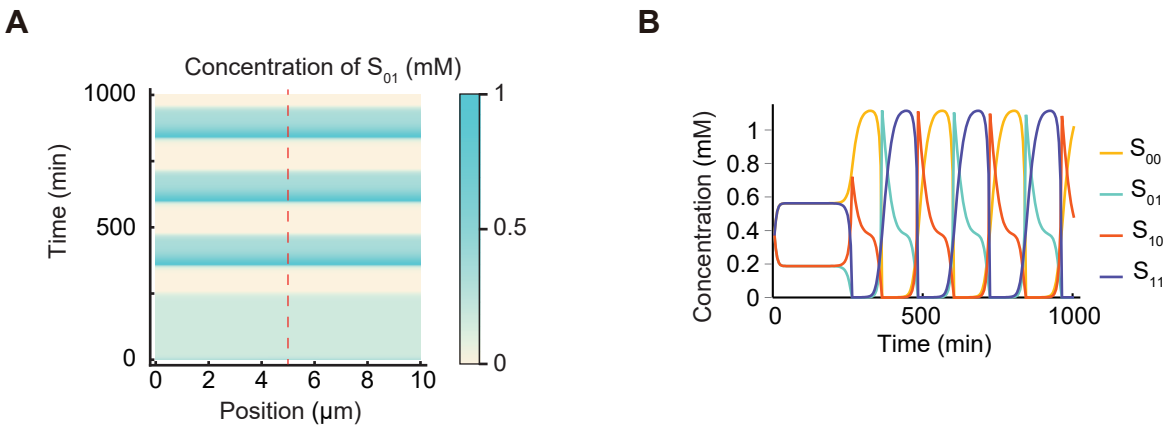

Figure S1. Two-site reversible phosphorylation can generate oscillation, related to **Figure 1**.

(**A**) An example of oscillation, showing the concentration of S_{01} along position and time. Vertical dotted line indicates the spatial section at the position of 5 μm shown in (**B**).

(**B**) A section of (**A**) at the position of 5 μm shows the limit cycle oscillation. Concentration of each substrate is plotted along with time.

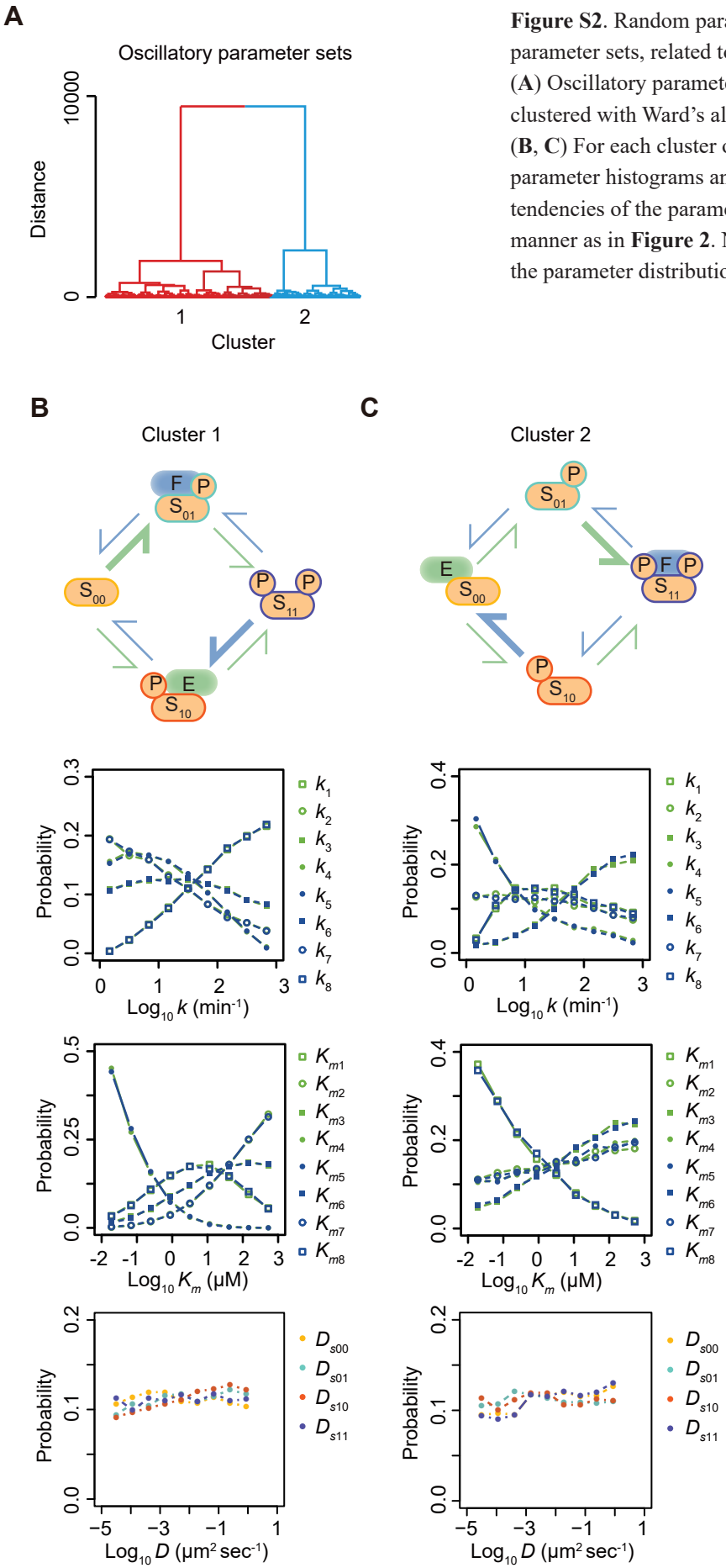

Figure S2. Random parameter search for oscillatory parameter sets, related to **Figure 2**.
(**A**) Oscillatory parameter sets found **Figure 2A** were clustered with Ward's algorithm.
(**B**, **C**) For each cluster of the oscillatory parameter sets, parameter histograms and a pictorial representation for tendencies of the parameters are depicted in the same manner as in **Figure 2**. No significant trend is found in the parameter distribution of diffusion coefficients.

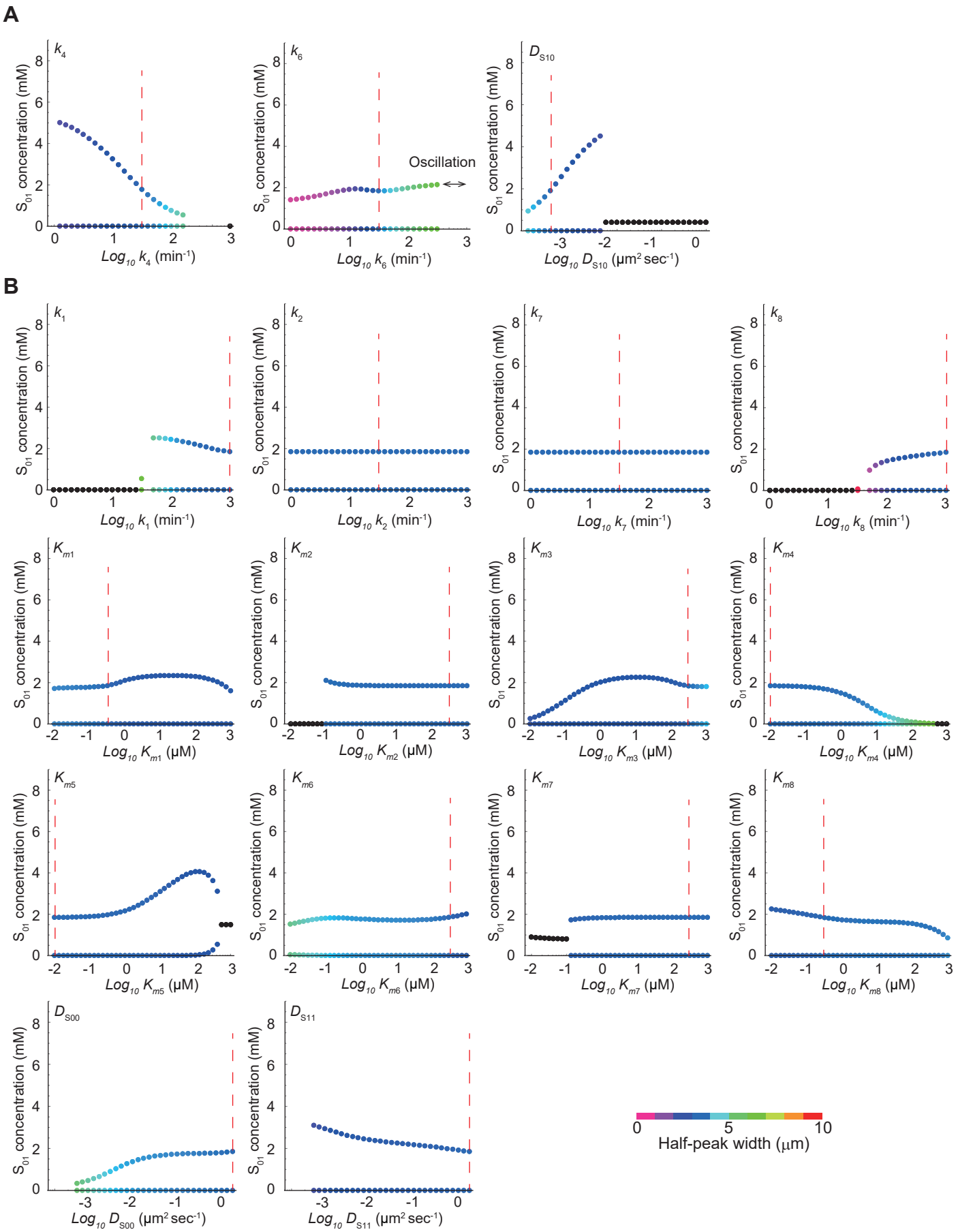

Figure S3. Bifurcation analysis to find the critical parameter for peak height and width, related to **Figure 3**.

The bifurcation analyses were conducted as shown in **Figure 3E**, and all the parameters except for the parameters shown in **Figure 3E** are shown in this figure. The symmetrical counterparts of parameters shown in **Figure 3E** are shown in (**A**), and the others are shown in (**B**).

See also **Table S1**.

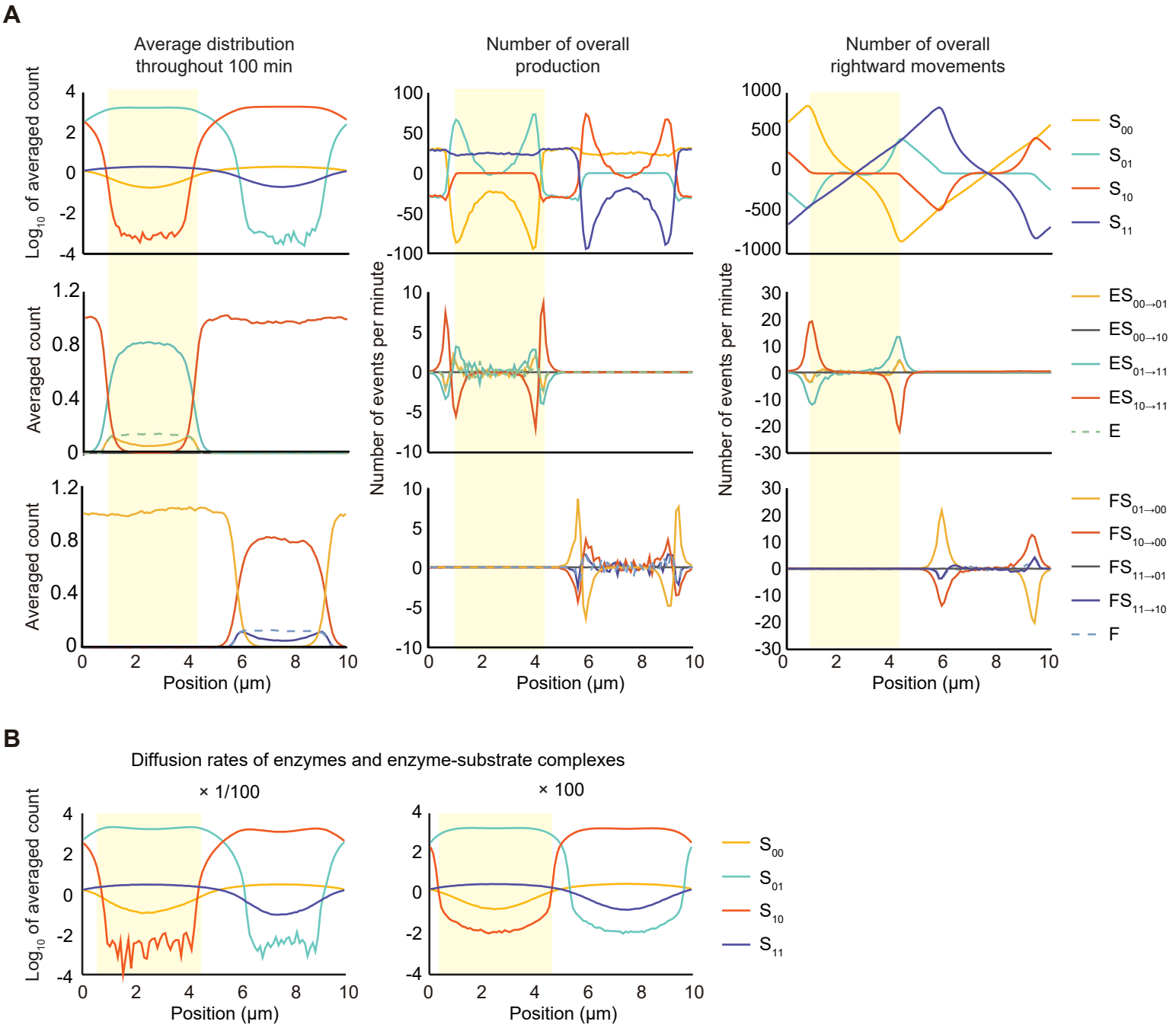

Figure S4. Stochastic simulation, related to **Figure 4**.

(**A**) The stochastic simulation was conducted with a parameter set corresponding to the representative parameter set for cluster 1 (see **Table S2**). For the final spatial pattern arising in the simulation, averaged distribution (left), overall production rate (middle), and overall rightward movements (right) are shown for each bin position. Distribution was averaged for 400 minutes after the establishment of spatial pattern. In the same time frame, overall production rate was evaluated by deducing depletion of the species of interest from its production, and overall movements were calculated for each bin by deducing leftward movements (from the next bin at right to the bin of interest) from the rightward movements (toward the next bin at right from the bin of interest). The distribution of enzyme-substrate complexes is explicitly calculated in SSA simulation. As these complexes are converted into products at a constant rate, their distributions are proportionate with the reaction rates calculated with PDE (see **Figure 3D**).

(**B**) Changing the diffusion rates of enzymes and enzyme-substrate complexes did not qualitatively alter the shape of the spatial pattern. Of the parameter values shown in **Table S2**, the diffusion rates of enzymes and enzyme-substrate complexes were altered either to one hundred times (1.667 $\mu m^2\ sec^{-1}$) or to one-hundredth (1.667×10^{-4} $\mu m^2\ sec^{-1}$) of the original value (0.01667 $\mu m^2\ sec^{-1}$). In both cases, distribution of each species was averaged for 100 minutes after the establishment of spatial pattern.

See also **Table S2**.

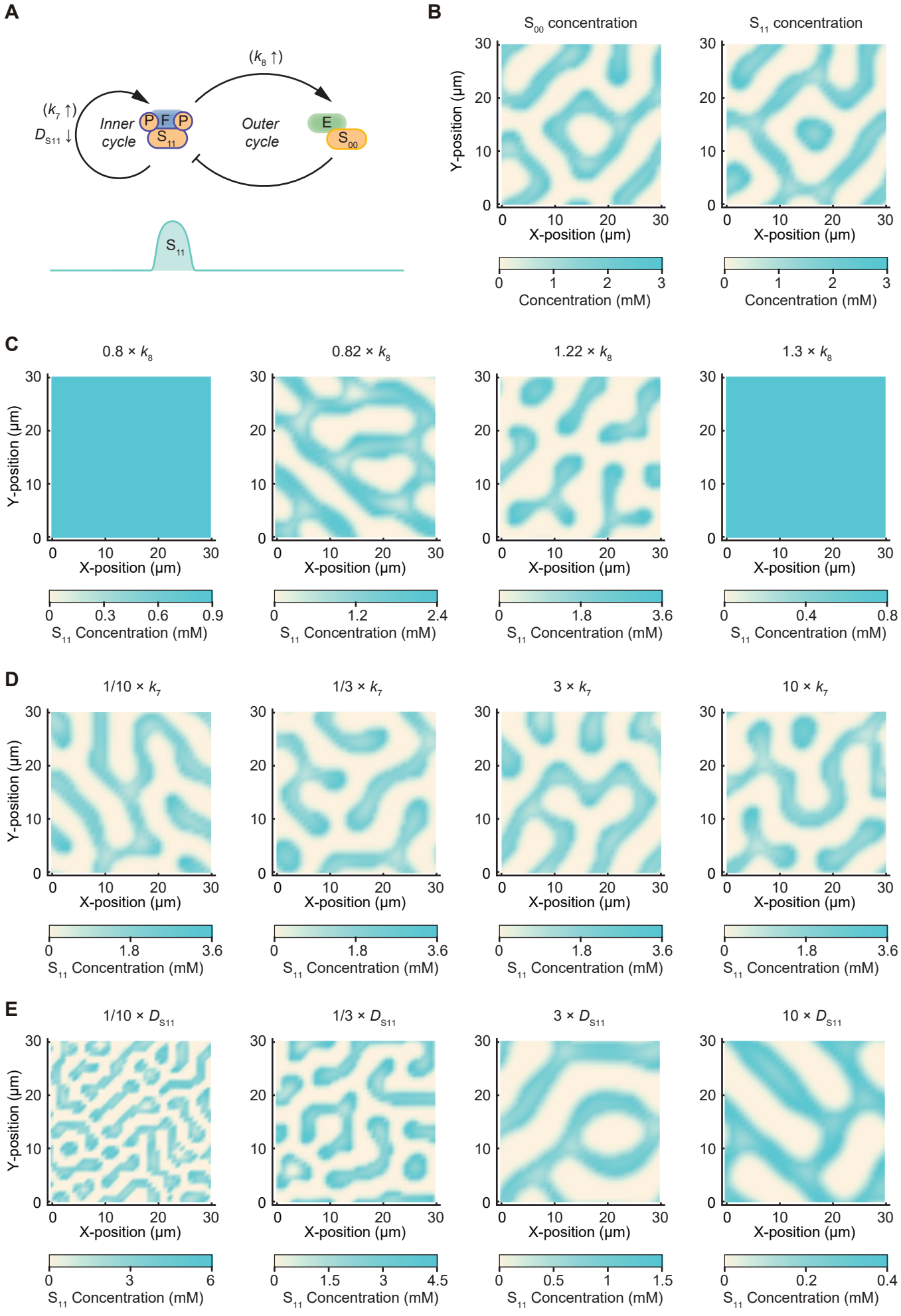

Figure S5. 2D pattern for the cluster 2-represenatative parameter set, related to **Figure 6**.

(**A**) Overall mechanism of spatial pattern formation and maintenance with cluster 2-representative parameter set similar to that with cluster 1-representative parameter set.

(**B**) 2D patterns emerged from cluster 2-representative parameter set.

(**C-E**) Modification of one of the parameter in the cluster 2-representative parameter set. Only the distributions of S_{11} are shown. See also **Table S1**.

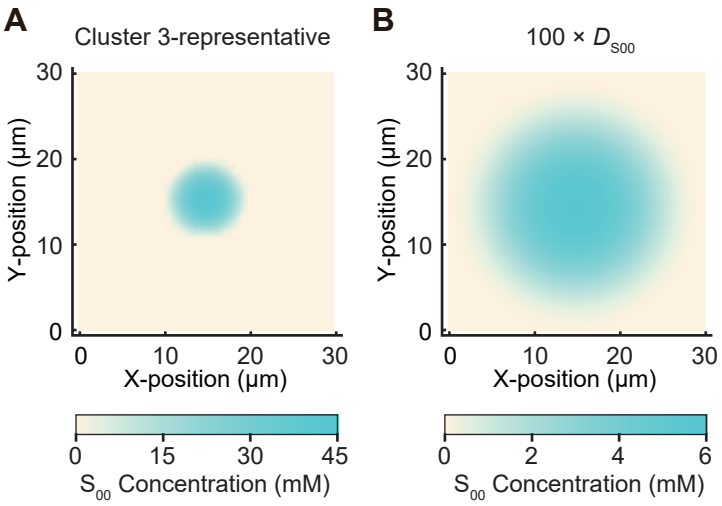

Figure S6. 2D pattern for the cluster 3-representative parameter set, related to **Figure 7**.
(**A**) Cluster 3-representative parameter set exhibits a small dot-shaped pattern, with most of the substance taking form of S_{00} and accumulating in the middle of the simulated area. The scale-independent emergence of single peak might be useful in circumstances where creating a single signal gradient in cell and subcellular structure is important, for example asymmetric cell division.
(**B**) Increasing D_{S00} caused broadening of the single peak, making a smooth gradient.
See also **Table S1**.

Table S1. Representative parameter sets of the four-component Michaelis-Menten model, related to **Figures 1, 3, 6, S3, S5,** and **S6**.

Parameter	Cluster 1	Cluster 2	Cluster 3
k_1 (min^{-1})	1000	30	30
k_2 (min^{-1})	30	30	30
k_3 (min^{-1})	30	1000	300
k_4 (min^{-1})	30	3	300
k_5 (min^{-1})	30	3	1000
k_6 (min^{-1})	30	1000	1000
k_7 (min^{-1})	30	30	300
k_8 (min^{-1})	1000	30	300
K_{m1} (μM)	0.3	0.01	20
K_{m2} (μM)	300	300	20
K_{m3} (μM)	300	0.3	0.02
K_{m4} (μM)	0.01	300	0.02
K_{m5} (μM)	0.01	300	30
K_{m6} (μM)	300	0.3	30
K_{m7} (μM)	300	300	1000
K_{m8} (μM)	0.3	0.01	1000
D_{S00} ($\mu m^2\ sec^{-1}$)	1.667	5×10^{-4}	1.667×10^{-5}
D_{S01} ($\mu m^2\ sec^{-1}$)	5×10^{-4}	1.667	1.667×10^{-3}
D_{S10} ($\mu m^2\ sec^{-1}$)	5×10^{-4}	1.667	1.667×10^{-3}
D_{S11} ($\mu m^2\ sec^{-1}$)	1.667	5×10^{-4}	1.667

Table S2. Representative parameter sets and collapsed parameter sets of the four-component model, related to **Figures 4**, **5**, and **S4**.

Parameter	Representative	Reaction motif collapsed	Binding motif collapsed	Diffusion motif collapsed	All motifs collapsed
k_{b1} (min^{-1} μM^{-1})	3367	274	249	3367	22
k_{b2} (min^{-1} μM^{-1})	0.1333	0.274	9.87	0.1333	22
k_{b3} (min^{-1} μM^{-1})	0.1333	0.274	9.87	0.1333	22
k_{b4} (min^{-1} μM^{-1})	4000	8210	9.87	4000	22
k_{b5} (min^{-1} μM^{-1})	4000	8210	9.87	4000	22
k_{b6} (min^{-1} μM^{-1})	0.1333	0.274	9.87	0.1333	22
k_{b7} (min^{-1} μM^{-1})	0.1333	0.274	9.87	0.1333	22
k_{b8} (min^{-1} μM^{-1})	3367	274	249	3367	22
k_{ub1}-k_{ub8} (min^{-1})	10	10	10	10	10
k_1 (min^{-1})	1000	72	1000	1000	72
k_2- k_7 (min^{-1})	30	72	30	30	72
k_8 (min^{-1})	1000	72	1000	1000	72
D_{S00} (μm^2 sec^{-1})	1.667	1.667	1.667	0.02	0.02
D_{S01} (μm^2 sec^{-1})	5×10^{-4}	5×10^{-4}	5×10^{-4}	0.02	0.02
D_{S10} (μm^2 sec^{-1})	5×10^{-4}	5×10^{-4}	5×10^{-4}	0.02	0.02
D_{S11} (μm^2 sec^{-1})	1.667	1.667	1.667	0.02	0.02
$D_{ES00\rightarrow01}$, $D_{ES00\rightarrow10}$, $D_{ES01\rightarrow11}$, $D_{ES10\rightarrow11}$, $D_{FS01\rightarrow00}$, $D_{FS10\rightarrow00}$, $D_{FS11\rightarrow01}$, $D_{FS11\rightarrow10}$, D_E, D_F (μm^2 sec^{-1})	0.01667	0.01667	0.01667	0.01667	0.01667

Table S3. Representative parameter set of the three-component Michaelis-Menten model, related to **Figure 7**.

Parameter	Representative
k_1 (min^{-1})	20
k_2- k_4 (min^{-1})	1000
K_{m1} (μM)	16
K_{m2} (μM)	0.01
K_{m3} (μM)	16
K_{m4} (μM)	10^3
D_{S0} ($\mu m^2\ sec^{-1}$)	1.667×10^{-5}
D_{S1} ($\mu m^2\ sec^{-1}$)	1.667×10^{-3}
D_{S2} ($\mu m^2\ sec^{-1}$)	1.667

Table S4. Representative parameter set of the three-component model converted to the full mass-action parameter, related to **Figure 7**.

Parameter	Representative
k_{b1} (min^{-1} μM^{-1})	1.875
k_{b2} (min^{-1} μM^{-1})	1.01×10^{5}
k_{b3} (min^{-1} μM^{-1})	63.13
k_{b4} (min^{-1} μM^{-1})	1.01
k_{ub1}-k_{ub4} (min^{-1})	10
k_1 (min^{-1})	20
k_2-k_4 (min^{-1})	10^{3}
D_{S0} (μm^2 sec^{-1})	1.667×10^{-5}
D_{S1} (μm^2 sec^{-1})	1.667×10^{-3}
D_{S2} (μm^2 sec^{-1})	1.667
D_{ES0}, D_{ES1}, D_{FS1}, D_{FS2}, D_E, D_F (μm^2 sec^{-1})	0.01667

SUPPLEMENTAL EXPERIMENTAL PROCEDURES

Software for computer simulation

Numerical integration of systems with PDE was carried out by using Mathematica software version 9.0 and 10.0 (Wolfram Research). Clustering of parameter sets was carried out by R software (The R project). The stochastic simulation was carried out by SSA (Gillespie, 1977) implemented in Cain software version 1.9 (http://cain.sourceforge.net/).

Reaction-diffusion equations for the single-site reversible phosphorylation

The reaction-diffusion equations for the reversible mono-phosphorylation scheme are described as below.

$$\frac{\partial}{\partial t}[S_0] = R_{\mathrm{S0}} + D_{\mathrm{S0}}\frac{\partial}{\partial x^2}[S_0], \tag{1.1}$$

$$\frac{\partial}{\partial t}[S_1] = R_{\mathrm{S1}} + D_{\mathrm{S1}}\frac{\partial}{\partial x^2}[S_1], \tag{1.2}$$

$$\frac{\partial}{\partial t}[E] = -R_{\mathrm{ES0}} + D_{\mathrm{E}}\frac{\partial}{\partial x^2}[E], \tag{1.3}$$

$$\frac{\partial}{\partial t}[F] = -R_{\mathrm{FS1}} + D_{\mathrm{F}}\frac{\partial}{\partial x^2}[F], \tag{1.4}$$

$$\frac{\partial}{\partial t}[ES_0] = R_{\mathrm{ES0}} + D_{\mathrm{ES0}}\frac{\partial}{\partial x^2}[ES_0], \tag{1.5}$$

$$\frac{\partial}{\partial t}[FS_1] = R_{\mathrm{FS1}} + D_{\mathrm{FS1}}\frac{\partial}{\partial x^2}[FS_1], \tag{1.6}$$

$$R_{\mathrm{S0}} = -k_{b1}[E][S_0] + k_{ub1}[ES_0] + k_2[FS_1], \tag{1.7}$$

$$R_{\mathrm{S1}} = -k_{b2}[F][S_1] + k_{ub2}[FS_1] + k_1[ES_0], \tag{1.8}$$

$$R_{\mathrm{ES0}} = k_{b1}[E][S_0] - k_{ub1}[ES_0] - k_1[ES_0], \tag{1.9}$$

$$R_{\mathrm{FS1}} = k_{b2}[F][S_1] - k_{ub2}[FS_1] - k_2[FS_1]. \tag{1.10}$$

For any given substance S, R_s stands for the "reaction term" denoting the phosphorylation and de-phosphorylation reactions. The "diffusion term," denoting each species' own free-diffusion process with the diffusion coefficient D_s, is described as following;

$$D_{\mathrm{S}}\frac{\partial}{\partial x^2}[S]. \tag{1.11}$$

$[S_0]$ and $[S_1]$ denote the concentrations of de- and mono-phosphorylated substrate. $[E]$ and $[F]$ denote the concentrations of kinase and phosphatase. $[ES_0]$ and $[FS_1]$ denote the concentrations of the enzyme-substrate complexes. Mass-action kinetics parameters, k_b, k_{ub}, and k, stand for the velocity coefficients of substrate-enzyme binding, unbinding, and phospho-group transfer. Properties of phosphorylation reactions are determined by k_{b1}, k_{ub1}, and k_1, while de-phosphorylation reactions are described by k_{b2}, k_{ub2}, and k_2.

Linear stability analysis

A reaction-diffusion system is said to have Turing instability or diffusion-induced instability when the uniform steady state is stable against a spatially homogeneous perturbation and unstable against a heterogeneous perturbation. To determine whether a given system can display Turing instability, linear stability analysis was conducted on the Jacobian matrix at the uniform steady state. For *n*-species system, the uniform steady state $\boldsymbol{S}^* = ([S_1^*], [S_2^*],,, [S_n^*])$ was evaluated either by solving $R_s = 0$ for every chemical species, or by running the simulation without the diffusion term until the system converges to $\boldsymbol{S}^*$. Suppose that the system resting at $\boldsymbol{S}^*$ receives a small perturbation approximated as $\sigma_m e^{ikx}$ (m = 1, 2,,, n), a sine function with wavenumber $k \geq 0$ and a small amplitude σ_m in spatial position *x*. Then the reaction-diffusion equations are reduced to;

$$\mathbf{0} = (\boldsymbol{R} - k^2\boldsymbol{D} - \lambda\boldsymbol{E})\boldsymbol{\Sigma}, \tag{2.1}$$

where

$$\boldsymbol{R} = \left\{r_{pq} \,\middle|\, 1 \leq p \leq n, 1 \leq q \leq n, r_{pq} = \frac{\partial}{\partial[S_p]}R_{\mathrm{S}q}(\boldsymbol{S}^*)\right\}, \tag{2.2}$$

$$\boldsymbol{D} = \left\{d_{pq} \,\middle|\, 1 \leq p \leq n, 1 \leq q \leq n, d_{pq} = \delta_{pq}D_{sp}\right\}. \tag{2.3}$$

$\boldsymbol{E}$ is an identity matrix and $\boldsymbol{\Sigma}$ is a vector with *n* members denoting a fluctuation from the steady state. Let λ_{max} be one of the solutions of the equation below, with the largest value of real part

$$|\boldsymbol{R} - k^2\boldsymbol{D} - \lambda\boldsymbol{E}| = 0. \quad (2.4)$$

For each $k \geq 0$, Re ($\lambda_{\max}$) represents growth rate of a perturbation of sine-wave shape with wavenumber k. Then the condition for Turing instability is as follows;

$$\mathrm{Re}(\lambda_{\max}) < 0 \text{ for } k = 0 \text{ and } \mathrm{Re}(\lambda_{\max}) > 0 \text{ for some } k > 0. \quad (2.5)$$

Absence of Turing instability in the single-site system

For the single-site reversible phosphorylation scheme described as the equations (1.1)-(1.10), the characteristic equation (2.4) becomes a sixth-degree polynomial equation of λ. From Routh-Hurwitz criterion (Edelstein-Keshet, 2005), this equation only yields solutions whose real part is negative, regardless of the parameter set. From the condition (2.5), possibility of Turing instability in this system is ruled out.

Reaction-diffusion equations for the four-state model

The four-state model shown in **Figure 1A** is described as below;

$$\frac{\partial}{\partial t}[S_{00}] = R_{\mathrm{S00}} + D_{\mathrm{S00}}\frac{\partial}{\partial x^2}[S_{00}], \quad (3.1)$$

$$\frac{\partial}{\partial t}[S_{01}] = R_{\mathrm{S01}} + D_{\mathrm{S01}}\frac{\partial}{\partial x^2}[S_{01}], \quad (3.2)$$

$$\frac{\partial}{\partial t}[S_{10}] = R_{\mathrm{S10}} + D_{\mathrm{S10}}\frac{\partial}{\partial x^2}[S_{10}], \quad (3.3)$$

$$\frac{\partial}{\partial t}[S_{11}] = R_{\mathrm{S11}} + D_{\mathrm{S11}}\frac{\partial}{\partial x^2}[S_{11}], \quad (3.4)$$

$$\frac{\partial}{\partial t}[E] = -R_{\mathrm{ES00}\to 01} - R_{\mathrm{ES00}\to 10} - R_{\mathrm{ES01}\to 11} - R_{\mathrm{ES10}\to 11} + D_{\mathrm{E}}\frac{\partial}{\partial x^2}[E], \quad (3.5)$$

$$\frac{\partial}{\partial t}[F] = -R_{\mathrm{FS01}\to 00} - R_{\mathrm{FS10}\to 00} - R_{\mathrm{FS11}\to 01} - R_{\mathrm{FS11}\to 10} + D_{\mathrm{F}}\frac{\partial}{\partial x^2}[F], \quad (3.6)$$

$$\frac{\partial}{\partial t}[ES_{00\to 01}] = R_{\mathrm{ES00}\to 01} + D_{\mathrm{ES00}\to 01}\frac{\partial}{\partial x^2}[ES_{00\to 01}], \quad (3.7)$$

$$\frac{\partial}{\partial t}[ES_{00\to 10}] = R_{\mathrm{ES00}\to 10} + D_{\mathrm{ES00}\to 10}\frac{\partial}{\partial x^2}[ES_{00\to 10}], \quad (3.8)$$

$$\frac{\partial}{\partial t}[ES_{01\to 11}] = R_{\mathrm{ES01}\to 11} + D_{\mathrm{ES01}\to 11}\frac{\partial}{\partial x^2}[ES_{01\to 11}], \quad (3.9)$$

$$\frac{\partial}{\partial t}[ES_{10\to 11}] = R_{\mathrm{ES10}\to 11} + D_{\mathrm{ES10}\to 11}\frac{\partial}{\partial x^2}[ES_{10\to 11}], \quad (3.10)$$

$$\frac{\partial}{\partial t}[FS_{01\to 00}] = R_{\mathrm{FS01}\to 00} + D_{\mathrm{FS01}\to 00}\frac{\partial}{\partial x^2}[FS_{01\to 00}], \quad (3.11)$$

$$\frac{\partial}{\partial t}[FS_{10\to 00}] = R_{\mathrm{FS10}\to 00} + D_{\mathrm{FS10}\to 00}\frac{\partial}{\partial x^2}[FS_{10\to 00}], \quad (3.12)$$

$$\frac{\partial}{\partial t}[FS_{11\to 01}] = R_{\mathrm{FS11}\to 01} + D_{\mathrm{FS11}\to 01}\frac{\partial}{\partial x^2}[FS_{11\to 01}], \quad (3.13)$$

$$\frac{\partial}{\partial t}[FS_{11\to 10}] = R_{\mathrm{FS11}\to 10} + D_{\mathrm{FS11}\to 10}\frac{\partial}{\partial x^2}[FS_{11\to 10}], \quad (3.14)$$

$$R_{\mathrm{S00}} = -(k_{b1} + k_{b2})[E][S_{00}] + k_{ub1}[ES_{00\to 01}] + k_{ub2}[ES_{00\to 10}] + k_5[FS_{01\to 00}] + k_6[FS_{10\to 00}], \quad (3.15)$$

$$R_{\mathrm{S01}} = -k_{b3}[E][S_{01}] - k_{b5}[F][S_{01}] + k_{ub3}[ES_{01\to 11}] + k_{ub5}[FS_{01\to 00}] + k_1[ES_{00\to 01}] + k_7[FS_{11\to 01}], \quad (3.16)$$

$$R_{\mathrm{S10}} = -k_{b4}[E][S_{10}] - k_{b6}[F][S_{10}] + k_{ub4}[ES_{10\to 11}] + k_{ub6}[FS_{10\to 00}] + k_2[ES_{00\to 10}] + k_8[FS_{11\to 10}], \quad (3.17)$$

$$R_{\mathrm{S11}} = -(k_{b7} + k_{b8})[F][S_{11}] + k_{ub7}[FS_{11\to 01}] + k_{ub8}[FS_{11\to 10}] + k_3[ES_{01\to 11}] + k_4[ES_{10\to 11}], \quad (3.18)$$

$$R_{\mathrm{ES00}\to 01} = k_{b1}[E][S_{00}] - k_{ub1}[ES_{00\to 01}] - k_1[ES_{00\to 01}], \quad (3.19)$$

$$R_{\mathrm{ES00}\to 10} = k_{b2}[E][S_{00}] - k_{ub2}[ES_{00\to 10}] - k_2[ES_{00\to 10}], \quad (3.20)$$

$$R_{\mathrm{ES01}\to 11} = k_{b3}[E][S_{01}] - k_{ub3}[ES_{01\to 11}] - k_3[ES_{01\to 11}], \quad (3.21)$$

$$R_{\mathrm{ES10}\to 11} = k_{b4}[E][S_{10}] - k_{ub4}[ES_{10\to 11}] - k_4[ES_{10\to 11}], \quad (3.22)$$

$$R_{\mathrm{FS01}\to 00} = k_{b5}[F][S_{01}] - k_{ub5}[FS_{01\to 00}] - k_5[FS_{01\to 00}], \quad (3.23)$$

$$R_{\mathrm{FS10}\to 00} = k_{b6}[F][S_{10}] - k_{ub6}[FS_{10\to 00}] - k_6[FS_{10\to 00}], \tag{3.24}$$

$$R_{\mathrm{FS11}\to 01} = k_{b7}[F][S_{11}] - k_{ub7}[FS_{11\to 01}] - k_7[FS_{11\to 01}], \tag{3.25}$$

$$R_{\mathrm{FS11}\to 10} = k_{b8}[F][S_{11}] - k_{ub8}[FS_{11\to 10}] - k_8[FS_{11\to 10}]. \tag{3.26}$$

For the massive random parameter search, Michaelis-Menten approximation was applied to reduce the number of variables. It assumes the enzyme-substrate binding and unbinding as having reached equilibrium, and reduces the set of reaction rate parameters $\{k_b, k_{ub}, k\}$ into $\{K_m, k\}$. K_m is called Michaelis constant given by

$$K_m = \frac{k_{ub}+k}{k_b}. \tag{3.27}$$

In the Michaelis-Menten -approximated version, the entire system is described by four equations, exchanging the reaction terms of (3.1)-(3.4) to the following;

$$R_{\mathrm{S00}} = -\left(\frac{k_1}{K_{m1}} + \frac{k_2}{K_{m2}}\right)[E][S_{00}] + \left(\frac{k_5}{K_{m5}}[S_{01}] + \frac{k_6}{K_{m6}}[S_{10}]\right)[F], \tag{3.28}$$

$$R_{\mathrm{S01}} = \left(\frac{k_1}{K_{m1}}[S_{00}] - \frac{k_3}{K_{m3}}[S_{01}]\right)[E] + \left(-\frac{k_5}{K_{m5}}[S_{01}] + \frac{k_7}{K_{m7}}[S_{11}]\right)[F], \tag{3.29}$$

$$R_{\mathrm{S10}} = \left(\frac{k_2}{K_{m2}}[S_{00}] - \frac{k_4}{K_{m4}}[S_{10}]\right)[E] + \left(-\frac{k_6}{K_{m6}}[S_{10}] + \frac{k_8}{K_{m8}}[S_{11}]\right)[F], \tag{3.30}$$

$$R_{\mathrm{S11}} = \left(\frac{k_3}{K_{m3}}[S_{01}] + \frac{k_4}{K_{m4}}[S_{10}]\right)[E] - \left(\frac{k_7}{K_{m7}} + \frac{k_8}{K_{m8}}\right)[F][S_{11}], \tag{3.31}$$

$$[E] = \frac{[E_{\mathrm{tot}}]}{1+\frac{[S_{00}]}{K_{m1}}+\frac{[S_{00}]}{K_{m2}}+\frac{[S_{01}]}{K_{m3}}+\frac{[S_{10}]}{K_{m4}}}, \tag{3.32}$$

$$[F] = \frac{[F_{\mathrm{tot}}]}{1+\frac{[S_{01}]}{K_{m5}}+\frac{[S_{10}]}{K_{m6}}+\frac{[S_{11}]}{K_{m7}}+\frac{[S_{11}]}{K_{m8}}}. \tag{3.33}$$

In our model, the total amount of enzymes are $[E_{\mathrm{tot}}] = [F_{\mathrm{tot}}] = 1$ μM and total amount of substrate was 1,500 μM unless otherwise indicated.

Random parameter search in the four-state model

The random parameter search in this paper aimed to find Turing instability-based spatial pattern formation and spatially homogeneous oscillation from reversible two-site phosphorylation. The 1D system size was set to 10 μm with a periodic boundary condition. Spatial pattern is defined by three criteria; 1) Turing instability, 2) temporal stability (i.e. temporal change of any species' concentration throughout a certain time is sufficiently small), and 3) spatial heterogeneity (at least one species shows a significant variance in its concentration distribution). Oscillation is characterized by two criteria; 4) temporal cyclicity, and 5) spatial homogeneity (i.e. spatial variance of any species' concentration throughout the simulated space is sufficiently small) of the chemical concentration.

For the four-state model, the following two steps were conducted to reduce calculation time. First, for each parameter set, a system without D was simulated under ordinary differential equations (ODEs). In the initial state, all the substrate exists as non-phosphorylated form (S_{00}) with the concentration of 1,500 μM. Kinase and phosphatase exist at the concentration of 1 μM. All the other substances have zero initial values. For each parameter set, calculation was continued at least until t = 1,000 min and at most until $t = 3 \times 10^8$ min. Parameter sets that showed either oscillatory behaviors or Turing instability were then allowed to proceed to the second step. The other parameter sets, converging to Turing-stable uniform steady state, or failing to converge within the calculation limit, were discarded. The concrete criteria of oscillation and Turing instability are as follows. For oscillation, the temporal trajectory of any of the simulated species must cross the same value three times. The two parts of trajectories sectioned by those three crossing points must display a high similarity with correlation coefficient greater than 0.99, and the peak amplitude of the two trajectories must not differ by greater than 1%. For Turing instability, the system must have converged to a steady state, and the determinant equation of Jacobian matrix at the steady state must have at least one solution with positive real part (see **Linear stability analysis**). This satisfies the criterion 1).

The second step uses the PDE with both reaction and diffusion term, and calculates the evolution of the system both along time and space. The initial condition of the PDE simulation was set as the final state of the ODE, hence mostly the same as the steady state of ODE. 0.1% fluctuation was added to the concentration of S_{00} for each spatial position. To prevent the memory from expiring, each simulation was split into several epochs with duration T. The first epoch has T = 2,500 min. Each epoch was extended to twice the duration of the previous epoch if the previous epoch was calculated without errors (e.g. probably the parameter set was near a bifurcation point and the behavior of the system was too stiff). If there was an error in the previous epoch, the same epoch was re-calculated with the duration shortened to half the duration of the previous epoch. If the error did not resolve even when the epoch size reaches T = 100 min or shorter, then the simulation was discarded.

The presence of stable spatial pattern is judged according to the following steps. As criterion 1)

is already established in the first step, the second step aims to establish criteria 2) and 3). After calculating each epoch, the concentration difference of two time points, T and $0.99T$, were evaluated at each position for each species. If the maximum of the concentration difference was less than 0.01 μM, then the simulation result was judged as having reached the equilibrium and met criterion 2). Then, for each of S_{00}, S_{01}, S_{10}, and S_{11}, the difference between its maximum and minimum concentration was calculated. If the largest one of the four values, named C_{max}, satisfies $C_{max} > 100$ μM then it was judged as having met criterion 3), hence the presence of stable spatial pattern. For oscillation, the time evolution at an arbitrary position in the space (in our simulation, $x = 2.5$ μm) must meet the same criteria as in the first step and be therefore considered as having met criterion 4). The system must also meet criterion 5) with $C_{max} < 0.01$ μM.

Clustering with collapsed symmetry

We used Ward's algorithm when clustering the spatial and oscillatory parameter sets. The distance matrices for the clustering were made with a metric to cancel out the inherent symmetries of the reaction scheme. The four-state model has a horizontal symmetry (e.g. exchanging the position of S_{01} and S_{10} conserves the overall structure) and a point-symmetry (e.g. exchanging the role of kinase and phosphatase conserves the overall structure). The distance between the two parameter sets P_1 and P_2 is defined as the minimum of the distances between P_1 and the four symmetrical images of P_2 – Min $\{P_1P_2, P_1P_3, P_1P_4, P_1P_5\}$ – where P_3 and P_4 are the horizontal and point-symmetrical transpositions, and P_5 is the combination of the two transpositions. P_3 is defined by transposing the parameters of P_2 as $k_1 \leftrightarrow k_2$, $k_3 \leftrightarrow k_4$, $k_5 \leftrightarrow k_6$, $k_7 \leftrightarrow k_8$, $K_{m1} \leftrightarrow K_{m2}$, $K_{m3} \leftrightarrow K_{m4}$, $K_{m5} \leftrightarrow K_{m6}$, $K_{m7} \leftrightarrow K_{m8}$, and $D_{S01} \leftrightarrow D_{S10}$. P_4 is defined by converting the parameters of P_2 as $k_1 \leftrightarrow k_8$, $k_2 \leftrightarrow k_7$, $k_3 \leftrightarrow k_6$, $k_4 \leftrightarrow k_5$, $K_{m1} \leftrightarrow K_{m8}$, $K_{m2} \leftrightarrow K_{m7}$, $K_{m3} \leftrightarrow K_{m6}$, $K_{m4} \leftrightarrow K_{m5}$, $D_{S00} \leftrightarrow D_{S11}$, and $D_{S01} \leftrightarrow D_{S10}$. The combination of two transpositions, P_5, is defined by the product of the above two steps. The order of the two transpositions does not affect the result, both being same as $k_1 \leftrightarrow k_7$, $k_2 \leftrightarrow k_8$, $k_3 \leftrightarrow k_5$, $k_4 \leftrightarrow k_6$, $K_{m1} \leftrightarrow K_{m7}$, $K_{m2} \leftrightarrow K_{m8}$, $K_{m3} \leftrightarrow K_{m5}$, $K_{m4} \leftrightarrow K_{m6}$, and $D_{S00} \leftrightarrow D_{S11}$.

Stochastic simulation

In Gillespie algorithm (Gillespie, 1977), two random numbers are generated for each iteration step; the first is to determine when the next process takes place, and the second is to determine what the process will be. Each random number is generated from a set of probability density functions that reflect the number of possible next processes and their ratio. In this study, the 1D spatial range (0-10 μM) with a periodic boundary condition was split into 100 identical bins. It is assumed that each bin is homogeneous and exchanges substances with the neighboring bins with a defined set of diffusion coefficients. By assuming diffusion as conversion process of a species in one bin into a species in the neighboring bins, diffusion can be treated in the same way as reaction.

For the simulations, the representative parameter sets in Michaelis-Menten-approximated version were converted to full mass-action parameter sets by fixing $k_{ub} = 10$ min^{-1} and solving the equation (3.27). The set of two parameters $\{K_m, k\}$ was thus converted to the three parameters $\{k_{ub}, k_b, k\}$ for each reaction. For the diffusion term, enzymes and enzyme-substrate complexes were all given the value of 1 μm^{2}min^{-1} (0.01667 μm^{2}sec^{-1}). See **Table S2** for the values.

Analysis of spatial pattern formation in the three-state model

When we consider kinase/phosphatase actions in two-site phosphorylation, we can choose from random or ordered models. The random model corresponds to the four-state model, while the ordered model corresponds to the three-state model. Although the ordered three-state model applies a strict constraint on the action of enzymes, it is mathematically simpler than the random model. On the other hand, the random four-state model is a biochemically more relaxed form and thus a more general model of two-site reversible modification. The three-state model with progressive two-site phosphorylation and the shared kinase and phosphatase is described as the equations below;

$$\frac{\partial}{\partial t}[S_0] = R_{S0} + D_{S0}\frac{\partial}{\partial x^2}[S_0], \tag{4.1}$$

$$\frac{\partial}{\partial t}[S_1] = R_{S1} + D_{S1}\frac{\partial}{\partial x^2}[S_1], \tag{4.2}$$

$$\frac{\partial}{\partial t}[S_2] = R_{S2} + D_{S2}\frac{\partial}{\partial x^2}[S_2], \tag{4.3}$$

$$\frac{\partial}{\partial t}[E] = -R_{ES0} - R_{ES1} + D_{E}\frac{\partial}{\partial x^2}[E], \tag{4.4}$$

$$\frac{\partial}{\partial t}[F] = -R_{FS1} - R_{FS2} + D_{F}\frac{\partial}{\partial x^2}[F], \tag{4.5}$$

$$\frac{\partial}{\partial t}[ES_0] = R_{ES0} + D_{ES0}\frac{\partial}{\partial x^2}[ES_0], \tag{4.6}$$

$$\frac{\partial}{\partial t}[ES_1] = R_{ES1} + D_{ES1}\frac{\partial}{\partial x^2}[ES_1], \tag{4.7}$$

$$\frac{\partial}{\partial t}[FS_1] = R_{FS1} + D_{FS1}\frac{\partial}{\partial x^2}[FS_1], \tag{4.8}$$

$$\frac{\partial}{\partial t}[FS_2] = R_{FS2} + D_{FS2}\frac{\partial}{\partial x^2}[FS_2], \tag{4.9}$$

$$R_{S0} = -k_{b1}[E][S_0] + k_{ub1}[ES_0] + k_3[FS_1], \tag{4.10}$$

$$R_{S1} = -k_{b3}[F][S_1] + k_{ub3}[FS_1] + k_1[ES_0] - k_{b2}[E][S_1] + k_{ub2}[ES_1] + k_4[FS_2], \tag{4.11}$$

$$R_{S2} = -k_{b4}[F][S_2] + k_{ub4}[FS_2] + k_2[ES_1], \tag{4.12}$$

$$R_{ES0} = k_{b1}[E][S_0] - k_{ub1}[ES_0] - k_1[ES_0], \tag{4.13}$$

$$R_{ES1} = k_{b2}[E][S_1] - k_{ub2}[ES_1] - k_2[ES_1], \tag{4.14}$$

$$R_{FS1} = k_{b3}[F][S_1] - k_{ub3}[FS_1] - k_3[FS_1], \tag{4.15}$$

$$R_{FS2} = k_{b4}[F][S_2] - k_{ub4}[FS_2] - k_4[FS_2]. \tag{4.16}$$

The names of the species and the indices of reaction parameters in the equations correspond to the ones in **Figure 7A**. The above set of nine PDEs was used in the stochastic simulation. With Michaelis-Menten approximation, the entire system is written by three variables for S_0, S_1, and S_2, exchanging the reaction terms of (4.1)-(4.3) to the following;

$$R_{S0} = -\frac{k_1}{K_{m1}}[E][S_0] + \frac{k_3}{K_{m3}}[F][S_1], \tag{4.17}$$

$$R_{S1} = \left(\frac{k_1}{K_{m1}}[S_0] - \frac{k_2}{K_{m2}}[S_1]\right)[E] + \left(\frac{k_4}{K_{m4}}[S_2] - \frac{k_3}{K_{m3}}[S_1]\right)[F], \tag{4.18}$$

$$R_{S2} = \frac{k_2}{K_{m2}}[E][S_1] - \frac{k_4}{K_{m4}}[F][S_2], \tag{4.19}$$

where

$$[E] = \frac{[E_{tot}]}{1+\frac{[S_0]}{K_{m1}}+\frac{[S_1]}{K_{m2}}}, \tag{4.20}$$

$$[F] = \frac{[F_{tot}]}{1+\frac{[S_1]}{K_{m3}}+\frac{[S_2]}{K_{m4}}}. \tag{4.21}$$

In the random parameter search with the three-state model, the same range for reaction rate constants (k), Michaelis constants (K_m), and diffusion coefficients (D) were used as with the four-state model. In the initial state, all the substrate exists as non-phosphorylated form (S_0) with the concentration of 1,500 μM. The kinase and phosphatase exist at the concentration of 1 μM. All the other substances have zero initial values. Each simulation for a given parameter set was composed of a sequence of epochs with the duration of T = 10,000 min. The calculation was continued at least for 1 epoch and at most for 20 epochs. If the result of simulation of an epoch met the following two conditions, it was determined that the simulation reached a stable spatial pattern; first, standard deviation of spatial distribution of at least one species' concentration must exceed 100 μM at the end of the epoch. Second, standard deviation of the temporal change of every species' concentration throughout the epoch must not exceed 0.1 μM at two points (x = 0 and x = 0.23).

Absence of Turing pattern in the two-site reversible phosphorylation model without enzyme sharing
With Michaelis-Menten approximation, it was shown that Turing pattern could never occur from the four-state scheme without enzyme sharing (i.e. all the reactions are carried out by different enzymes). The reaction-diffusion equations of the four-state model without enzyme sharing are described as below instead of (3.28) through (3.33);

$$R_{S00} = -\frac{k_1}{K_{m1}+[S_{00}]}[E_{tot1}][S_{00}] - \frac{k_2}{K_{m2}+[S_{00}]}[E_{tot2}][S_{00}] + \frac{k_5}{K_{m5}+[S_{01}]}[F_{tot1}][S_{01}] + \frac{k_6}{K_{m6}+[S_{10}]}[F_{tot2}][S_{10}], \tag{5.1}$$

$$R_{S01} = \frac{k_1}{K_{m1}+[S_{00}]}[E_{tot1}][S_{00}] - \frac{k_3}{K_{m3}+[S_{01}]}[E_{tot3}][S_{01}] - \frac{k_5}{K_{m5}+[S_{01}]}[F_{tot1}][S_{01}] + \frac{k_7}{K_{m7}+[S_{01}]}[F_{tot3}][S_{11}], \tag{5.2}$$

$$R_{S10} = \frac{k_2}{K_{m2}+[S_{00}]}[E_{tot2}][S_{00}] - \frac{k_4}{K_{m4}+[S_{10}]}[E_{tot4}][S_{10}] - \frac{k_6}{K_{m6}+[S_{10}]}[F_{tot2}][S_{10}] + \frac{k_8}{K_{m8}+[S_{10}]}[F_{tot4}][S_{11}], \tag{5.3}$$

$$R_{S11} = \frac{k_3}{K_{m3}+[S_{01}]}[E_{tot3}][S_{01}] + \frac{k_4}{K_{m4}+[S_{10}]}[E_{tot4}][S_{10}] - \frac{k_7}{K_{m7}+[S_{11}]}[F_{tot3}][S_{11}] - \frac{k_8}{K_{m8}+[S_{11}]}[F_{tot4}][S_{11}]. \tag{5.4}$$

For this set of equations, possibility of Turing instability was algebraically ruled out with any combination

of reaction parameters and total amounts of enzymes; all the Routh-Hurwitz coefficients are positive with no change of signs. Possibility of Turing instability in the three-state model without enzyme sharing was also ruled out by setting $k_2 = k_4 = k_6 = k_8 = 0$. For the three-state model, we attempted the same analysis for all possible patterns of enzyme sharing, using Routh-Hurwitz criterion. It was shown that Turing pattern is possible when two phosphorylating reactions share the kinase, or when two de-phosphorylating reactions share the phosphatase, or when the both are satisfied at the same time; in all the other cases, spatial pattern emergence was ruled out. The results of analyses in Michaelis-Menten-approximated schemes are not directly applicable to the full mass-action scheme, especially where the fundamental premise for the approximation fails (e.g. where the total amount of enzymes and substrates are at the similar order). We did not conduct the same analysis on the full mass-action scheme, as it became unfeasible within our limit of computation power.

Algebraic condition for Turing instability in the three-state model with shared kinase and phosphatase

In the case of three-state reversible phosphorylation scheme with a shared kinase and a shared phosphatase, the value of each r_{pq} in definition (2.2) are as follows;

$$r_{11} = -\frac{k_1 K_{m1} K_{m2} [E_{\mathrm{tot}}](K_{m2}+[S_1{}^*])}{(K_{m1}K_{m2}+K_{m2}[S_0{}^*]+K_{m1}[S_1{}^*])^2} < 0, \tag{6.1}$$

$$r_{12} = \frac{k_3 K_{m3} K_{m4} [F_{\mathrm{tot}}](K_{m2}[S_0{}^*]+K_{m1}(K_{m2}+[S_1{}^*]))^2 (K_{m4}+[S_2{}^*])+k_1 K_{m1} K_{m2} [E_{\mathrm{tot}}][S_0{}^*](K_{m4}[S_1{}^*]+K_{m3}(K_{m4}+[S_2{}^*]))^2}{(K_{m2}[S_0{}^*]+K_{m1}(K_{m2}+[S_1{}^*]))^2 (K_{m4}[S_1{}^*]+K_{m3}(K_{m4}+[S_2{}^*]))^2} > 0, \tag{6.2}$$

$$r_{13} = -\frac{k_3 K_{m3} K_{m4} [\mathrm{F_{tot}}][S_1{}^*]}{\left(K_{m4}[S_1{}^*]+K_{m3}(K_{m4}+[S_2{}^*])\right)^2} < 0, \tag{6.3}$$

$$r_{31} = -\frac{k_2 K_{m1} K_{m2} [E_{\mathrm{tot}}][S_1{}^*]}{\left(K_{m2}[S_0{}^*]+K_{m1}(K_{m2}+[S_1{}^*])\right)^2} < 0, \tag{6.4}$$

$$r_{32} = \frac{k_4 K_{m3} K_{m4} [F_{\mathrm{tot}}][S_2{}^*](K_{m2}[S_0{}^*]+K_{m1}(K_{m2}+[S_1{}^*]))^2 + k_2 K_{m1} K_{m2} [E_{\mathrm{tot}}](K_{m1}+[S_0{}^*])(K_{m4}[S_1{}^*]+K_{m3}(K_{m4}+[S_2{}^*]))^2}{(K_{m2}[S_0{}^*]+K_{m1}(K_{m2}+[S_1{}^*]))^2 (K_{m4}[S_1{}^*]+K_{m3}(K_{m4}+[S_2{}^*]))^2} > 0, \tag{6.5}$$

$$r_{33} = -\frac{k_4 K_{m3} K_{m4} [F_{\mathrm{tot}}](K_{m3}+[S_1{}^*])}{\left(K_{m4}[S_1{}^*]+K_{m3}(K_{m4}+[S_2{}^*])\right)^2} < 0. \tag{6.6}$$

The Jacobian matrix can be rewritten using positive numbers,

$$F_{11} = -r_{11}, F_{12} = r_{12}, F_{13} = -r_{13}, F_{31} = -r_{31}, F_{32} = r_{32}, F_{33} = -r_{33}, \tag{6.7}$$

Then,

$$\boldsymbol{R} - k^2 \boldsymbol{D} - \lambda \boldsymbol{E} = \begin{pmatrix} -F_{11} - D_{\mathrm{S0}} * k^2 - \lambda & F_{12} & -F_{13} \\ F_{11} + F_{31} & -F_{12} - F_{32} - D_{\mathrm{S1}} * k^2 - \lambda & F_{33} + F_{13} \\ -F_{31} & F_{32} & -F_{33} - D_{\mathrm{S2}} * k^2 - \lambda \end{pmatrix} \tag{6.8}$$

Then (2.4) becomes:

$$a_0 \lambda^3 + a_1 \lambda^2 + a_2 \lambda + a_3 = 0, \tag{6.9}$$

where

$$a_0 = -1 < 0, \tag{6.10}$$

$$a_1 = k^2(-D_{\mathrm{S0}} - D_{\mathrm{S1}} - D_{\mathrm{S2}}) - F_{11} - F_{12} - F_{32} - F_{33} < 0, \tag{6.11}$$

$$a_2 = k^4(-D_{\mathrm{S0}}D_{\mathrm{S1}} - D_{\mathrm{S1}}D_{\mathrm{S2}} - D_{\mathrm{S0}}D_{\mathrm{S2}}) + k^2\big(-D_{\mathrm{S2}}(F_{11}+F_{12}+F_{32}) - D_{\mathrm{S1}}(F_{11}+F_{33}) - D_{\mathrm{S0}}(F_{12}+F_{32}+F_{33})\big) + F_{12}F_{31} + F_{13}F_{31} + F_{13}F_{32} - F_{11}F_{32} - F_{11}F_{33} - F_{12}F_{33}, \tag{6.12}$$

$$a_3 = k^2(-k^4 D_{\mathrm{S0}}D_{\mathrm{S1}}D_{\mathrm{S2}} - k^2\big(D_{\mathrm{S0}}D_{\mathrm{S2}}(F_{12}+F_{32}) + D_{\mathrm{S1}}(D_{\mathrm{S2}}F_{11} + D_{\mathrm{S0}}F_{33})\big) + D_{\mathrm{S0}}(F_{13}F_{32} - F_{12}F_{33}) + D_{\mathrm{S1}}(F_{13}F_{31} - F_{11}F_{33}) + D_{\mathrm{S2}}(F_{12}F_{31} - F_{11}F_{32})). \tag{6.13}$$

As the first step for solving the analytic condition (2.5) for the system to have Turing instability, the condition for stability at $k = 0$ is investigated. Since a_3 becomes zero for $k = 0$, equation (6.9) becomes

$$\lambda(a_0\lambda^2 + a_1\lambda + a_2) = 0, \tag{6.14}$$

where $\lambda = 0$ is a trivial solution arising from mass-conservation. Its corresponding eigenvector points to the direction that all the substance increases at the same time, breaching the mass-conservation itself. This is biochemically meaningless and is omitted from consideration. The equation (6.14) is then reduced to;

$$a_0\lambda^2 + a_1\lambda + a_2 = 0. \tag{6.15}$$

For both of the two solutions of this equation to have negative real parts, $a_2 < 0$ ($k = 0$) must be met. This is equivalent to;

$$F_{12}F_{31} + F_{13}F_{31} + F_{13}F_{32} - F_{11}F_{32} - F_{11}F_{33} - F_{12}F_{33} < 0. \tag{6.16}$$

Next, the condition for instability for some $k > 0$ is investigated. From Routh-Hurwitz criterion, the signs of the 4 Routh-Hurwitz coefficients must not be the same. These coefficients are a_0, a_1, a_3 and b_1, which is written as

$$b_1 = a_2 - \frac{a_0 a_3}{a_1}. \tag{6.17}$$

Substitution of equation (6.17) by k, D_{S0}, D_{S1}, D_{S2}, F_{11}, F_{12}, F_{13}, F_{31}, F_{32}, and F_{33} yields a polynomial with only negative coefficients. This proves that b_1 is always negative. Combined with equations (6.10) and (6.11), indicating that both a_0 and a_1 are negative, Turing instability can be made possible only when $a_3 > 0$. We investigated the condition to satisfy

$$a_3' = a_3/k^2 = -k^4 D_{S0}D_{S1}D_{S2} - k^2\left(D_{S0}D_{S2}(F_{12} + F_{32}) + D_{S1}(D_{S2}F_{11} + D_{S0}F_{33})\right) + D_{S0}(F_{13}F_{32} - F_{12}F_{33}) + D_{S1}(F_{13}F_{31} - F_{11}F_{33}) + D_{S2}(F_{12}F_{31} - F_{11}F_{32}) > 0. \tag{6.18}$$

The coefficients of k^2 and k^4 are both negative, making a_3' monotonically decrease. Therefore, the only case we have to consider in the periodic boundary condition for the spatial range is $k = 2\pi$.

From the above analysis, a given parameter set must satisfy all the conditions in the following steps in order to result in a spatial pattern formation, all of which can be checked algebraically;

(1) Evaluate $\boldsymbol{S}^*$ = ([S_0^*], [S_1^*], [S_2^*]) by solving the zero point of reaction terms of reaction-diffusion equations. In the three-state model with Michaelis-Menten approximation, this yields a cubic equation and thus algebraically solvable. From $\boldsymbol{S}^*$, extract the solutions that are within a chemically possible range (i.e. real and positive). This yields either one or three different solutions.
(2) Ensure that $\boldsymbol{S}^*$ is a stable steady state without diffusion. This can be done by solving $|\boldsymbol{R} - \lambda\boldsymbol{E}| = 0$ and checking that Re (λ_{max}) < 0. If $\boldsymbol{S}^*$ is unstable, it must be omitted from the later analysis.
(3) For $k = 2\pi$, if any of the following two tautologous conditions are met, then the given parameter set would result in a spatial pattern: i) $a_3 > 0$, or ii) Re (λ_{max}) > 0 where λ is given by solving a cubic equation $|\boldsymbol{R} - k^2\boldsymbol{D} - \lambda\boldsymbol{E}| = 0$.

A detailed analysis on the pattern formation in two-dimensional space for cluster 2 and 3

Though the cluster 1 and 2 are highly similar with 90-degree rotation of the reaction scheme (see **Figure 2C** and **2D**) and similar regulation of pattern shape in 2D space was observed with the representative parameter set for cluster 2, they are not exactly the same. For example, the peak height is resilient against the changes in one parameter responsible for the "inner" cycle in cluster 2 (i.e. k_7). The difference can be attributed to the different parameter topology between cluster 1 and 2 because these clusters are not perfectly symmetric: for example, in the cluster 1, high affinity between S_{01} and phosphatase promotes the reaction $S_{01} \rightarrow S_{00}$ that counteracts the overall clockwise bias in the reaction rate. On the other hand, in the cluster 2, high affinity between S_{00} and kinase promoters the reaction from $S_{00} \rightarrow S_{01}$ that supports the overall clockwise reaction bias.

In the following explanation, the parameters of cluster 2 are compared with those of cluster 1 with clockwise 90-degree rotation – for example, S_{00} of cluster 1 is compared with S_{01} of cluster 2 and k_1 of cluster 1 is compared with k_3 of cluster 2. With the representative parameter set of cluster 1, the onset of the "inner cycle" (i.e. $S_{01} \rightarrow S_{00}$) is mediated by phosphatase, while the onset of the "outer cycle" (i.e. $S_{01} \rightarrow S_{11}$) is mediated by kinase. S_{01} can thus proceed either to the "inner" cycle or the "outer" cycle at a similar order of reaction rate. On the other hand, with cluster 2-representative parameter set, the two possible reactions for S_{11} (i.e. $S_{11} \rightarrow S_{01}$ and $S_{11} \rightarrow S_{10}$) are both catalyzed by phosphatase. The direction in which S_{11} proceeds is determined by the ratio of K_{m7} and K_{m8}. As K_{m8} is overwhelmingly smaller than K_{m7}, S_{11} predominantly proceeds to the "outer cycle." Thus, k_8 in cluster 2, the first component of the "outer" cycle, plays a much more crucial role to the maintenance of spatial pattern than k_3 in cluster 1 does. A small alteration of k_8 significantly changes the pattern width; only 18% decrease results in an S_{11}-dominant pattern and 22% increase produces an S_{00}-dominant pattern (**Figure S5C**). The heavy dependence to the "outer" cycle makes the pattern collapse easily with only 20% decrease or 30% increase (**Figure S5C**). On the other hand, k_7 in cluster 2, the first component of the "inner" cycle, does not contribute so much to the

maintenance of spatial pattern formation as k_5 does in cluster 1, thus altering k_7 has little effect on the pattern shape (**Figure S5D**). As diffusion process is independent from the chemical reaction, alteration of D_{S11} produced mostly the same result as altering D_{S01} in cluster 1 (**Figure S5E**); decrease of D_{S11} resulted in higher peaks with a narrower pitch, while its increase produced an opposite effect with lower peaks with a wider pitch.

With the representative parameter of cluster 3, almost all the substances accumulate at the single position in the form of S_{00}. Increasing D_{S00}, the diffusion rate of the accumulating species, resulted in a wider peak with a lower peak value (**Figure S6A** and **B**).

SUPPLEMENTAL REFERENCE

Edelstein-Keshet, L. (2005). Mathematical models in biology, Classics edn (Philadelphia: Society for Industrial and Applied Mathematics).